

Relaxation Time Correlation NMR for Mechanochemical *in-situ* Reaction Monitoring of Metal-Organic Frameworks

*Madeleine E. Leger,^{ab} Jiangfeng Guo,^b Bryce MacMillan,^b Hatem M. Titi,^c Tomislav Friščić,^c
Barry A. Blight,^{a*} and Bruce Balcom^{a,b*}*

^a Department of Chemistry, University of New Brunswick, Fredericton, New Brunswick, E3B 5A3, Canada

^b UNB MRI Centre, Department of Physics, University of New Brunswick, Fredericton, New Brunswick, E3B 5A3, Canada

^c Department of Chemistry, McGill University, Montreal, Quebec, H3A 0B8, Canada

RECEIVED DATE (to be automatically inserted after your manuscript is accepted if required according to the journal that you are submitting your paper to)

* Corresponding author: bjb@unb.ca, b.blight@unb.ca

ABSTRACT:

We present a new methodology for real-time observation of mechanochemical transformations, based on a magnetic resonance method in which T_1 - T_2^* relaxation time correlation maps are used to track the formation of the popular metal-organic framework (MOF) materials Zn-MOF-74 and ZIF-8. This two-dimensional (2D) relaxation correlation measurement is a new method utilizing simple saturation recovery to obtain a T_1 - T_2^* spectrum representing different hydrogen environments. The 2D T_1 - T_2^* results show a change in signal amplitudes, and their coordinates, within the plots as the reaction progresses, confirming reaction completion. Static solid samples are usually considered difficult to measure because of their short-lived T_2^* signal and their common non-exponential decay. Using a new processing method, the signal from samples with non-exponential decay was quantified. The importance of key parameters such as the instrument deadtime, the recovery times, and magnetic field strength for the measurement of solids with a short-lived signal is established. This novel magnetic resonance measurement is important since it provides a simple and easy way to analyse an entire solid reaction mixture within its reaction vessel.

KEYWORDS: T_1 - T_2^* , nuclear magnetic resonance, relaxation time, saturation recovery, free induction decay, mechanochemistry, sinc-gaussian decay, metal-organic frameworks.

1. Introduction

Mechanochemistry, i.e. chemical reactions induced and/or sustained through grinding, milling, shearing or other types of mechanical agitation, has emerged as a popular and highly versatile method for synthesizing molecules and materials in the absence of bulk solvents.¹ The ability to circumvent the need for bulk solvents, at the same time providing access to chemical reactions that are fast, proceed at room temperature, and can provide access to molecules and materials challenging to obtain through other means, makes mechanochemistry a highly attractive and ‘greener’ alternative to more conventional solvent-based synthetic approaches. The scope of possible reactions by mechanochemical activation is widespread, with recent reviews and reports outlining mechanochemical approaches to organic,^{2,3} inorganic,^{4,5} organometallic,⁶ supramolecular,⁷⁻⁹ and coordination^{10,11} chemistry, as well as a range of advanced materials such as metal-organic frameworks, nanomaterials, and more. Mechanochemical transformations open the door to new synthetic opportunities¹² such as the formation of unusual products, trapping of typically unstable intermediates, and the enhanced selectivity of products¹³ while also serving as an important tool for the reduction of reaction times.¹²

The mechanics of mechanochemical milling remain poorly understood,^{14,15} with attempts^{16,17} to elucidate the underlying physicochemical process often involving extensive and systematic investigations of temperature and pressure, including real-time approaches, as well as screening of milling frequency, sample-to-volume ratio, ball diameter, material of the milling assembly, presence and properties of liquid and/or polymer additives, and other parameters.^{12,18-21} It is noteworthy that in-depth and real-time monitoring of reactions by thermography,²²⁻²⁴ manometric studies,²⁵ synchrotron powder X-ray diffraction (PXRD),²⁶⁻³⁰ Raman spectroscopy,^{21,31,32} and different combinations of these³³⁻³⁷ have shown great progress in our

ability to monitor mechanochemical processes without the need to disrupt the reaction. Despite rapid and exciting successes, the *in situ* mechanochemistry monitoring approaches are still in their infancy with challenges yet to be overcome. One of these is the difficulty to obtain reliable insight into the course of mechanochemical reactions through acquiring data over a limited/small and inhomogeneous sampling area/volume, which can lead to low quality data that is difficult to interpret.³⁸ Ex-situ monitoring continues to be an appropriate method for product analysis since the final product of a mechanochemical reaction is often stable and inert in nature.¹

Magnetic resonance (MR) is an incredibly varied and expanding field. While it is best known for its uses in chemical spectroscopic analysis^{39,40} and in the medical field,^{41,42} MR can be used in many other capacities. Specifically, relaxation time experiments are currently used to analyse materials such as porous materials (e.g. rock cores)⁴³⁻⁴⁵ and foods.⁴⁶⁻⁴⁹ Most of these analyses involve the measurement of relaxation time parameters such as the longitudinal (T_1) and transverse (T_2) relaxation times. T_1 - T_2 correlation analysis has proven to be a very important experiment in MR. The T_1 - T_2 measurement is ideal for samples with long T_2 lifetimes. While this measurement is appropriate for a variety of samples, most solid materials have T_2 values too short-lived to acquire useful data. Recently, Marreiros et al.⁵⁰ published their work demonstrating MOF adsorption using T_1 - T_2 measurements but have identified one of the core challenges to be measuring samples, such as solids, with short-lived T_2 signal.

A new measurement utilizing T_1 - T_2^* relaxation-time correlation maps reported by Enjilela *et al.*⁵¹ has great merit for solid samples. T_2^* relaxation is driven by T_2 relaxation which is typically very short in solid samples. The T_1 - T_2^* method is simple and combines saturation recovery with free induction decays. The minimum observation time of the T_1 - T_2^* method is only limited by the instrument deadtime, which makes it ideal to measure rigid samples with short T_2^* lifetimes. T_1 -

T_2^* measurements have been used to distinguish water and oil in shales,^{52,53} and to classify coal samples,⁵⁴ but they have yet been applied to monitor the development of solid-state chemical reactions.

In this work, we propose a novel approach for analysis of mechanochemical reactions *in situ*, using MR relaxation time correlation measurements to measure hydrogen environments of mechanochemical reactions. Our research provides a new and transformative method of analysis that will eliminate the need for material transfer, with all the attendant benefits. In such a scenario, the entire mechanochemical process, from synthesis to analysis, would take place in the milling container, with analysis being completed on the entire reaction mixture. Metal-organic frameworks (MOFs)⁵⁵⁻⁵⁷ serve as ideal examples for the herein presented proof-of-principle study because of the significant changes in ligand conformation / topology and therefore, in hydrogen environment. Increasingly, mechanochemical synthesis is a popular method for MOF formation,⁵⁸⁻⁶⁵ with several MOFs already having been produced on a large scale by extrusion.⁶⁶ In this work, we have used as a model system the synthesis of the well-known MOF material Zn-MOF-74^{67,68} (also known as CPO-27^{69,70}), with special interest paid to the formation of a reaction intermediate and evident colour change. Also, an in-situ T_1 - T_2^* relaxation correlation analysis method is successfully demonstrated using the mechanochemical synthesis of another popular MOF, the zeolitic imidazolate framework ZIF-8.^{67,71}

2. Experimental

2.1 Chemicals

Zinc oxide (99%), 2-methylimidazole (99%), zinc acetate dihydrate (98%), and 2,5-dihydroxyterephthalic acid (98%), were purchased from Sigma Aldrich. All reactants were used without further purification.

2.2 MR method

In solid-state time domain MR analysis, an instrument with a very short deadtime must be utilized to capture the short T_2^* component found in solid materials. A 4.7 T vertical-bore superconducting magnet (Cryomagnetics) and a Redstone HF NMR spectrometer console (Tecmag) equipped with a Doty DS1-874 ^1H RF probe (Doty Scientific) were utilized. Samples were either transferred to a glass vial for analysis or kept in the lab-made Teflon jar used during milling (see Supporting Material (SM), section S1). A large amount of sample (gram scale) was required to acquire enough signal to overcome the background signal from the probe.

Parameters specific to these measurements included a dwell time of 400 ns, a pulse length of 5 μs , a total of 8 scans, and the acquisition of 4096 time domain points for all samples. Some pulse specific parameters included a recycle delay of 175 s for the free induction decay (FID) sequence, and a set of 40 recovery times ranging from 15 μs to 99 s for the saturation recovery pulse sequence. The receiver gain (RG) depended on the intensity of signal measured from each sample and the values varied from 25 to 100. The deadtime was 4 μs .

The data was collected using simple FID and saturation recovery (SM, section S1). Total measurement time took approximately 20 minutes for the individual FID measurement and 1 hour 48 minutes for the saturation recovery measurement. A MATLAB program employing code from

the program by the Schlumberger-Doll Research Center was utilized to process the data to generate the T_1 - T_2^* time correlation maps. This program assumed the signal change to be purely exponential. For non-exponential data processing, a new T_1 - T_2^* analysis method was employed.⁷² A detailed explanation of the MR measurement is in the supplementary materials (SM, section S1).

2.3 Synthetic methods and characterization

The model mechanochemical preparation of Zn-MOF-74 and ZIF-8 followed the ball milling procedures previously established by Julien *et al.*³⁰ and Beldon *et al.*,⁷³ respectively. For the mechanosynthesis of Zn-MOF-74, 6.67 mmol of zinc oxide (543 mg), 3.33 mmol of 2,5-dihydroxyterephthalic acid (660 mg), and 0.75 mL of water were milled in a 15 mL polymethyl methacrylate (PMMA) jar for 90 minutes at 30 Hz. For the milling synthesis of ZIF-8, 3.75 mmol of zinc oxide (305 mg), 7.5 mmol of 2-methylimidazole (616 mg), and 0.2 μ L/mg of N,N-dimethylformamide (DMF) (175 μ L) were added to a lab-made Teflon jar, with two big 10 mm zirconia balls. In a Retsch MM400 mixer mill, the jar was shaken at 30 Hz for 60 minutes.

The identities of the products were confirmed through powder X-ray diffraction (PXRD) patterns that were collected on a Bruker D2 PHASER diffractometer. The PXRD patterns of the solid reactants were obtained with a Bruker D8 Advance spectrometer. Thermogravimetric analysis (TGA) data was collected on a TGA 5500 Discovery instrument. Scanning Electron Microscope (SEM) images and Energy Dispersive X-ray Spectroscopy (EDS) data were collected on a JEOL JSM-6400 Scanning Electron Microscope equipped with an EDAX Genesis 4000 Energy Dispersive X-ray analyser. Detailed methodology for PXRD, TGA, SEM, and EDS can be found in the supplementary materials (SM, section S1).

Results and Discussion

3.1 Reactions and Characterization

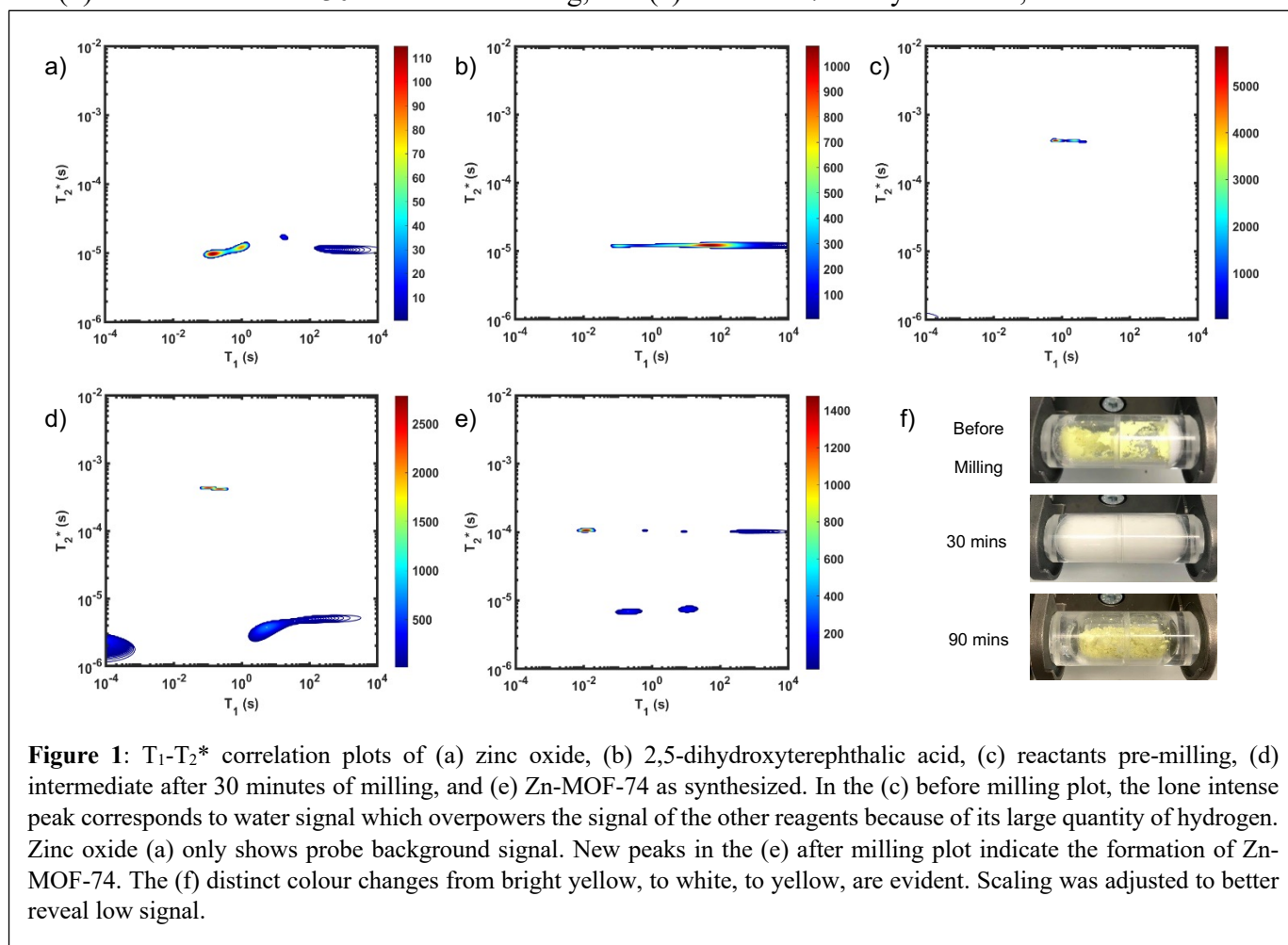
The mechanochemical syntheses of the two model MOFs by milling were analysed by MR relaxation time measurements. The synthesis of Zn-MOF-74 followed the procedure established by Julien *et al.*,³⁰ consisting of liquid-assisted grinding (LAG)⁷⁴ ZnO, 2,5-dihydroxyterephthalic acid, and water together. The material Zn-MOF-74 is a representative of the M-MOF-74 family of materials (M = a divalent metal cation) which is particularly interesting for their excellent stability, as well as gas adsorption and catalysis abilities.⁷⁵ The second model reaction involved the synthesis of ZIF-8 and followed the procedure previously shown by Beldon *et al.*,⁷³ which involved the LAG of ZnO and 2-methylimidazole in the presence of DMF as the liquid additive. The framework ZIF-8 has been extensively studied for its promising capabilities in gas separation, sensing, and catalysis due to its excellent chemical and thermal stability.⁶⁷ Detailed mechanisms of the mechanochemical syntheses of Zn-MOF-74³⁰ and ZIF-8^{26,76} materials have been published. The reaction mixtures were characterized by PXRD (SM, see section S5), SEM images and corresponding EDS data (SM, see section S6), TGA (SM, see section S7), as well as MR correlation plots.

3.2 Mechanochemical synthesis of Zn-MOF-74

The formation of Zn-MOF-74 by mechanochemical milling is particularly interesting for its distinct colour changes and documented appearance of an intermediate.³⁰ The use of clear PMMA milling jars permitted observation of these changes during reaction milling (Figure 1f). The starting mixture appears bright yellow due to the presence of 2,5-dihydroxyterephthalic acid (H₄dhta), but it quickly transforms to a pale yellow, and eventually a white paste. White material is evidence of the intermediate, Zn(H₂O)₂(H₂dhta), being formed. The yellow hue of the Zn-MOF-

74 product is visible as the viscous mixture suddenly transforms into a powder, which is a sign of reaction completion. The final product is a dry dull yellow powder. The quick transition from liquid mixture to dry product is reminiscent of the observations made by the James group⁷⁷ in organic mechanosynthesis and could be related to the moisture sequestration of Zn-MOF-74.⁷⁸

Figure 1 demonstrates tracking of the progress of the Zn-MOF-74 mechanosynthesis using our new MR method. Distinct changes in the peaks are visible between the reactant, pre-milling, and after milling plots which is consistent with the formation of the targeted MOF product. Correlation plots of (a) zinc oxide and (b) 2,5-dihydroxyterephthalic acid were measured using different scaling to the other plots to account for low sample signal. The plots of (c) reactants pre-milling, (d) intermediate after 30 minutes of milling, and (e) Zn-MOF-74 as synthesized, all contained the



same amount of material and hydrogen, but loss of product did occur during transfer to the measurement vial. The plots show variable scaling to better reveal low signal.

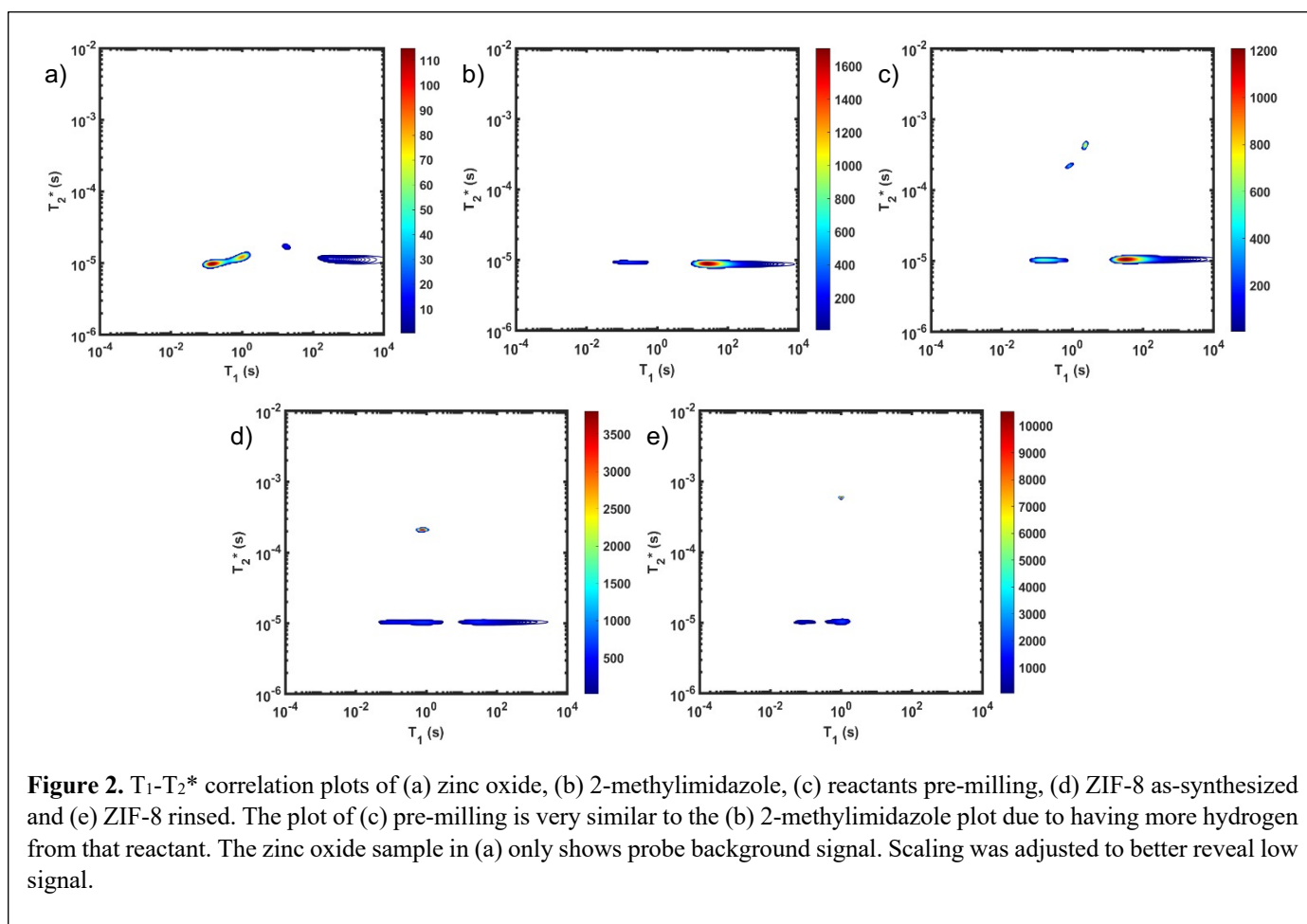
The plot of zinc oxide contains no hydrogen signal, which is apparent in Figure 1a. Any observed signal can be ascribed to background signal from the probe, and possible minor impurities in the commercially sourced zinc oxide sample. The 2,5-dihydroxyterephthalic acid correlation plot (Figure 1b) shows a single short T_2^* value at 12.1 μs . The T_1 value at the center of the peak is at 47.7 s and the very left side of the peak is at 0.11 s. The FID shows a clear sinc-gaussian decay (SM, see section S3).

The starting materials before milling include 0.75 mL of water, which is apparent in the 2D plot (Figure 1c). Water has long T_1 and T_2 lifetimes due to significant mobility in the liquid state. The noted intermediate was captured after 30 minutes of milling, shown in Figure 1d. The water peak is still very evident, with new peaks appearing in the bottom two corners of the plot. Formation of Zn-MOF-74 (Figure 1e) shows multiple new peaks, attributed to assembly of the periodic porous solid. The T_1 of the major peak on the upper left of the plot is at 12 ms. The T_1 of the two peaks on the bottom are 0.20 s and 11.2 s. While the T_2^* values are 6.8 μs , 7.6 μs and 106 μs . The smaller less intense peaks trailing off to the right at the longer T_2^* are most likely artifacts. Water adsorption of the porous Zn-MOF-74 product explains the change in water peak.⁷⁸ The relaxation time values for all these samples are summarized in table S1 in the supplementary information.

3.3 Mechanochemical formation of ZIF-8 with *in-situ* MR Analysis

The important advantage to highlight with the T_1 - T_2^* MR measurement is the ability to complete in-situ analysis of the entire reaction mixture. This differs greatly from other in-situ

methods, as X-rays or scattering lasers are limited to localized analysis. The synthesis of ZIF-8 served as our example (Figure 2). The reaction was milled in a small lab-made Teflon jar with two small zirconia balls. The materials, made from Teflon and zirconia, permitted the MR measurement due to low hydrogen content. This allows the reaction to be milled and analysed without ever having to open the milling vessel. The measurements of (a) zinc oxide and (b) 2-methylimidazole employed a bigger sample than reaction scale to account for low sample signal. The plots of (c) reactants pre-milling, (d) ZIF-8 as synthesized and (e) ZIF-8 rinsed, all contained the same amount of material and therefore, hydrogen. The plots show variable scaling to better reveal low signal.



As noted before, the zinc oxide signal (Figure 2a) consists mostly of background signal from the probe and vial. The 2-methylimidazole 2D plot (Figure 2b) indicates one short T_2^* signal at 9.1 μs . The major peak has a T_1 value of 24.9 s. We posit that the smaller less intense peak with a T_1 of 0.17 s comes from background signal. For 2-methylimidazole, the decay signal is sinc-gaussian (SM, see section S3).

Starting materials were mixed and spectra collected prior to milling (Figure 2c). It displays a very similar profile to 2-methylimidazole (Figure 2b), indicating that most of the hydrogen signal is coming from that reactant. The plot corresponding to the ZIF-8 product (Figure 2d) consists of three distinct peaks. The top intense peak has a T_1 value of 0.78 s and T_2^* of 210 μs , evidence of the DMF used to facilitate the reaction and molecular water formed as a by-product. The ZIF-8 peak just underneath it has a similar T_1 value of 0.83 s and a shorter T_2^* of 10.5 μs . The third peak with a short T_2^* value of 10.5 μs but longer T_1 value of 28.8 s represents leftover 2-methylimidazole. This is supported by figure 2e, which shows the product after rinsing and drying overnight under vacuum where the 2-methylimidazole peak is absent. The remaining signal has similar relaxation time values as the previous plot. The relaxation time values for all these samples are summarized in Table S1 in the supplementary materials. It is worth noting that some ZnO phase does remain in the mixture, and though MR inactive, is visible in the PXRD.

3.4 Exponential vs non-exponential analysis

Two types of processing exist for T_1 - T_2^* data sets. First, the simpler and best-known option is to process all the data as if the magnetization evolution curves are all exponentials. This type of processing is simple and is commonly used, and the MATLAB program is already developed by the Schlumberger-Doll Research Center. The program is user-friendly and only requires a few parameters to be manually changed. We utilized this method to process the results in figures 1 and

2. The disadvantage is that many rigid samples, like many of our solid samples, display non-exponential gaussian or sinc-gaussian T_2^* decay curves (SM, see section S3).⁷⁹ The sinc-gaussian non-exponential T_2^* decay in the time domain occurs due to a distribution of Pake doublets in the frequency domain.⁸⁰

This results in non-exponential curves being processed as exponential curves. Although this can be an issue for quantification, the results shown by Guo et al. demonstrate that the plots using this approximation yield similar relaxation time values to the non-exponential processing results.⁷² Exponential processing is a suitable method for species identification and differentiation, but it is not suitable for quantification of the samples. This is further supported in figure 3 where we compare exponential and non-exponential processing of ZIF-8 synthesis where the exponential processing peaks are very similar to the graphs generated from the non-exponential processing method (SM, see section S4).

Non-exponential processing is vital for quantifying signal intensity by its accurate fitting of gaussian or sinc-gaussian curves. A novel processing method reported by Guo et al. processes the non-exponential part of the decay and the exponential part separately to generate the correlation plots to achieve accurate quantifiable results of non-exponential decays, or a combination of exponential and non-exponential decays.⁷² MR measurements are linear measurements and can be demonstrated as such. In our study, the hydrogen signal of materials before milling and after milling is conserved as established in both of our MOF reactions milled in our lab-made Teflon jars. The synthesis of ZIF-8 and its conservation of signal is demonstrated in figure 3.

Figure 3a and 3b demonstrate the correlation plot results using exponential decay processing while figure 3a-f demonstrate results using non-exponential processing. As mentioned previously, the resulting relaxation time values between the two types of processing methods are very similar

but, without non-exponential processing, accurate quantification of the samples is impossible. Figure 3 compares the two methods. In the pre-milling figures 3a and 3c, the most intense peak is located at a T_1 of 30.9 s for exponential processing and 28.8 s for the non-exponential processing. The T_2^* is the same at 10.5 μ s for both types of processing. In the post-milling figures 3b and 3d, the liquid peak at a longer T_2^* is situated at 0.78 s and 210 μ s for both types of processing, for T_1 and T_2^* respectively. The ZIF-8 peak, at the shortest T_1 and T_2^* values, has a T_1 of 0.83 s and T_2^* of 10.5 μ s for exponential and a T_1 of 0.90 s and T_2^* of 20.0 μ s for non-exponential processing. The third peak corresponds to leftover 2-methylimidazole. The relaxation times are summarized in table S2 of the supplementary information.

The easiest and most accurate method for quantification involves the back-extrapolation of 1D T_2^* data sets obtained by FID to obtain the time-zero value intensity (figure 3e and 3f). In this case, the decay of pre-milling and ZIF-8 as synthesized both contain a gaussian component and an exponential component. In these FID plots, the black line represents the raw data while the red line indicates the fitting. The reactants pre-milling has a signal intensity of 9.10×10^4 and the ZIF-8 as synthesized of 9.69×10^4 , establishing conservation of hydrogen signal before and after milling. The 2D plots processed by non-exponential fitting can also be used to calculate total signal intensity (figure 3c and 3d). Using this method, the pre-milling has a signal intensity of 9.70×10^4 and the ZIF-8 as synthesized of 1.05×10^5 . The values are still similar enough to conclude a linear measurement, but the signal intensity determined from the FID data will always be more accurate.

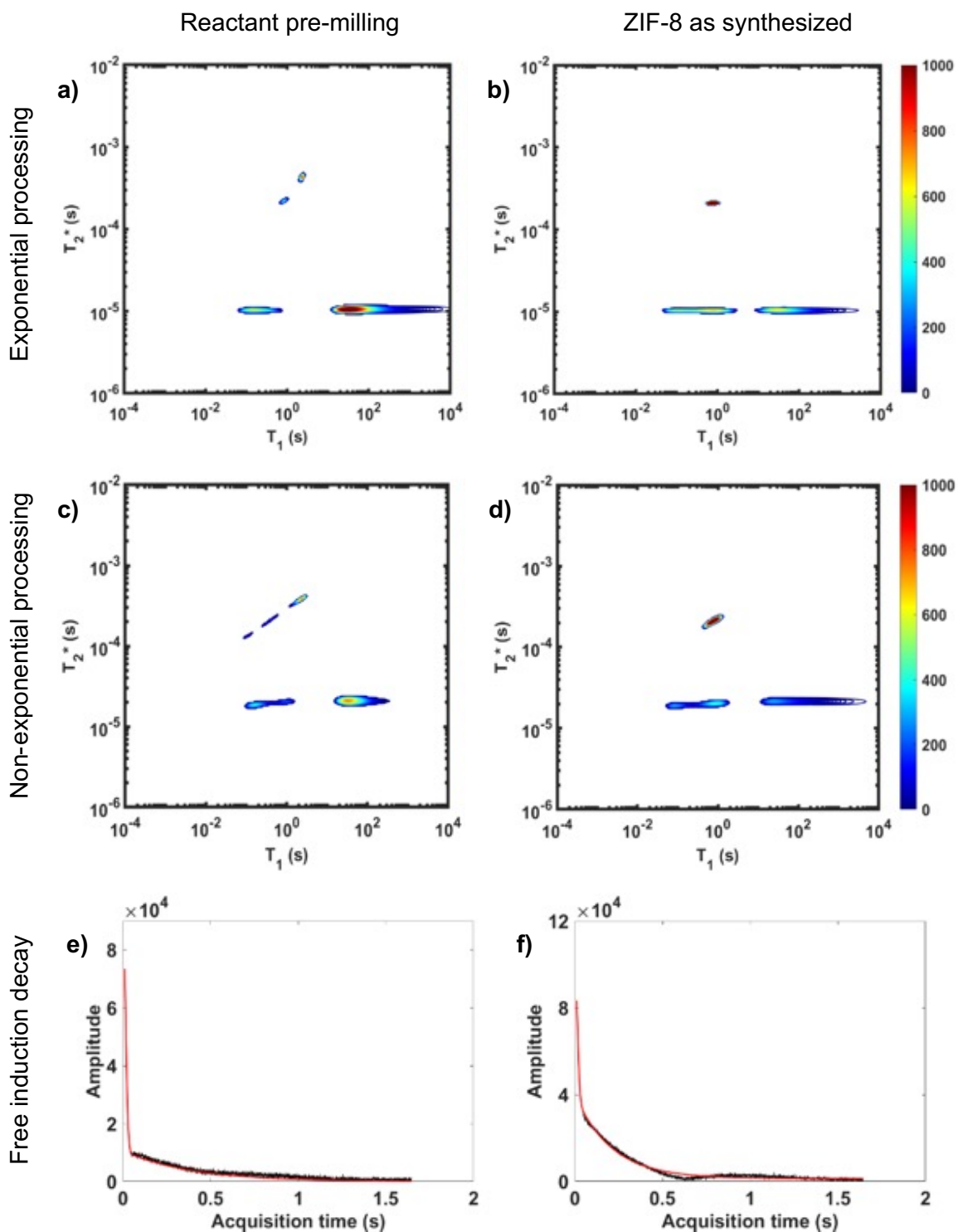


Figure 3: Comparison of exponential and non-exponential processing of ZIF-8 synthesis. Plots a and b are T_1 - T_2^* correlation plots using exponential processing while c and d used non-exponential processing. The plots are described as the following: (a) reactants pre-milling with exponential processing, (b) ZIF-8 as synthesized with exponential processing, (c) reactants pre-milling with non-exponential processing, and (d) ZIF-8 as synthesized with non-exponential processing. The 1D plots of free induction decay of T_2^* using non-exponential processing of (e) ZIF-8 as synthesized and (f) ZIF-8 purified. Both 1D plots show a combination of two types of decay: gaussian and exponential decay.

3. Conclusions

We describe for the first time, a new method of in-situ solid-state analysis of mechanochemical reactions using T_1 - T_2^* relaxation correlation plots, where whole-reaction mixtures can be evaluated in the reaction vessel by readily available short deadtime MR equipment. Simple saturation recovery sequence was employed to acquire T_1 - T_2^* data from the solid samples. A short instrument deadtime and long recovery times were needed to acquire the short-lived signal and capture the long T_1 values. The reactions of Zn-MOF-74 and ZIF-8 were completed in a ball mill and monitored using T_1 - T_2^* correlation maps. Significant differences in relaxation correlation peaks were used to determine the completion of the reaction, confirmed by PXRD data and TGA. The T_1 - T_2^* measurement provides an easy, versatile, and solvent-free process especially useful for mechanochemical reactions and other chemical transformations, such as the formation of aggregates for example. This new method can ultimately be applied to many industrial processes and materials, as already seen with shales and coals.⁵²⁻⁵⁴ Moving forward, we envisage the use of an economical lower-field benchtop NMR instrument that will allow the measurement to be shorter, more accessible, and more versatile without the need for specially engineered equipment for data collection. T_1 is greatly influenced by magnetic field, and a lower field magnet would shorten the T_1 , therefore shortening the measurement time greatly. The analysis method will be further improved by shortening the measurement time by utilising a Look Locker sequence. This would permit the acquisition of multiple FIDs per saturation, instead of only acquiring one FID per saturation using our current saturation recovery measurement. A probe without background signal would be helpful and allow the measurement of smaller scale reactions with less hydrogen content. To expand the scope of the measurement, we are now exploring $T_{1\rho}$ - T_2^* correlation measurements.⁷²

References

- (1) James, S. L.; Adams, C. J.; Bolm, C.; Braga, D.; Collier, P.; Friščić, T.; Grepioni, F.; Harris, K. D. M.; Hyett, G.; Jones, W.; Krebs, A.; Mack, J.; Maini, L.; Orpen, A. G.; Parkin, I. P.; Shearouse, W. C.; Steed, J. W.; Waddell, D. C. Mechanochemistry: Opportunities for New and Cleaner Synthesis. *Chem. Soc. Rev.* **2012**, *41* (1), 413–447. <https://doi.org/10.1039/C1CS15171A>.
- (2) Tan, D.; Friščić, T. Mechanochemistry for Organic Chemists: An Update. *Euro. J. Org. Chem.* **2018**, *2018* (1), 18–33. <https://doi.org/10.1002/ejoc.201700961>.
- (3) Egorov, I. N.; Santra, S.; Kopchuk, D. S.; Kovalev, I. S.; Zyryanov, G. v.; Majee, A.; Ranu, B. C.; Rusinov, V. L.; Chupakhin, O. N. Ball Milling: An Efficient and Green Approach for Asymmetric Organic Syntheses. *Green Chem.* **2020**, *22* (2), 302–315. <https://doi.org/10.1039/c9gc03414e>.
- (4) Tan, D.; Garcí, F. Main Group Mechanochemistry: From Curiosity to Established Protocols. *Chem. Soc. Rev.* **2019**, *48* (8), 2274–2292. <https://doi.org/10.1039/c7cs00813a>.
- (5) Moores, A. Bottom up, Solid-Phase Syntheses of Inorganic Nanomaterials by Mechanochemistry and Aging. *Curr. Opin. Green Sust. Chem.* **2018**, *12*, 33–37. <https://doi.org/10.1016/j.cogsc.2018.05.004>.
- (6) Rightmire, N. R.; Hanusa, T. P. Advances in Organometallic Synthesis with Mechanochemical Methods. *Dalton Trans.* **2016**, *45* (6), 2352–2362. <https://doi.org/10.1039/c5dt03866a>.
- (7) Braga, D.; Maini, L.; Grepioni, F. Mechanochemical Preparation of Co-Crystals. *Chem. Soc. Rev.* **2013**, *42* (18), 7638–7648. <https://doi.org/10.1039/c3cs60014a>.
- (8) Bose, A.; Mal, P. Mechanochemistry of Supramolecules. *Beilstein J. Org. Chem.* **2019**, *15*, 881–900. <https://doi.org/10.3762/bjoc.15.86>.
- (9) Friščić, T. Supramolecular Concepts and New Techniques in Mechanochemistry: Cocrystals, Cages, Rotaxanes, Open Metal-Organic Frameworks. *Chem. Soc. Rev.* **2012**, *41* (9), 3493–3510. <https://doi.org/10.1039/c2cs15332g>.
- (10) Mottillo, C.; Friščić, T. Advances in Solid-State Transformations of Coordination Bonds: From the Ball Mill to the Aging Chamber. *Molecules* **2017**, *22* (1). <https://doi.org/10.3390/molecules22010144>.
- (11) Friščić, T.; Halasz, I.; Štrukil, V.; Eckert-Maksić, M.; Dinnebier, R. E. Clean and Efficient Synthesis Using Mechanochemistry: Coordination Polymers, Metal-Organic Frameworks and Metallodrugs. *Croat. Chem. Acta* **2012**, *85* (3), 367–378. <https://doi.org/10.5562/cca2014>.
- (12) Howard, J. L.; Cao, Q.; Browne, D. L. Mechanochemistry as an Emerging Tool for Molecular Synthesis: What Can It Offer? *Chem. Sci.* **2018**, *9* (12), 3080–3094. <https://doi.org/10.1039/c7sc05371a>.
- (13) Hernández, J. G.; Bolm, C. Altering Product Selectivity by Mechanochemistry. *J. of Org. Chem.* **2017**, *82* (8), 4007–4019. <https://doi.org/10.1021/acs.joc.6b02887>.

- (14) Užarević, K.; Halasz, I.; Friščić, T. Real-Time and in Situ Monitoring of Mechanochemical Reactions: A New Playground for All Chemists. *Journal of Physical Chemistry Letters* **2015**, *6* (20), 4129–4140. <https://doi.org/10.1021/acs.jpcclett.5b01837>.
- (15) Colacino, E.; Carta, M.; Pia, G.; Porcheddu, A.; Ricci, P. C.; Delogu, F. Processing and Investigation Methods in Mechanochemical Kinetics. *ACS Omega* **2018**, *3* (8), 9196–9209. <https://doi.org/10.1021/ACSOMEGA.8B01431>.
- (16) Michalchuk, A. A. L.; Tumanov, I. A.; Drebuschak, V. A.; Boldyreva, E. v. Advances in Elucidating Mechanochemical Complexities via Implementation of a Simple Organic System. *Faraday Discuss.* **2014**, *170*, 311–335. <https://doi.org/10.1039/c3fd00150d>.
- (17) McKissic, K. S.; Caruso, J. T.; Blair, R. G.; Mack, J. Comparison of Shaking versus Baking: Further Understanding the Energetics of a Mechanochemical Reaction. *Green Chem.* **2014**, *16* (3), 1628–1632. <https://doi.org/10.1039/c3gc41496e>.
- (18) Schmidt, R.; Burmeister, C. F.; Baláž, M.; Kwade, A.; Stolle, A. Effect of Reaction Parameters on the Synthesis of 5-Arylidene Barbituric Acid Derivatives in Ball Mills. *Organic Process Research & Development* **2015**, *19* (3), 427–436. <https://doi.org/10.1021/op5003787>.
- (19) Schmidt, R.; Scholze, H. Martin; Stolle, Achim. Temperature Progression in a Mixer Ball Mill. *International Journal of Industrial Chemistry* **2016**, *7*, 181–186. <https://doi.org/10.1007/s40090-016-0078-8>.
- (20) Stolle, A.; Schmidt, R.; Jacob, K. Scale-up of Organic Reactions in Ball Mills: Process Intensification with Regard to Energy Efficiency and Economy of Scale. *Faraday Discussions* **2014**, *170*, 267–286. <https://doi.org/10.1039/c3fd00144j>.
- (21) Julien, P. A.; Malvestiti, I.; Friščić, T. The Effect of Milling Frequency on a Mechanochemical Organic Reaction Monitored by in Situ Raman Spectroscopy. *Beilstein Journal of Organic Chemistry* **2017**, *13*, 2160–2168. <https://doi.org/10.3762/bjoc.13.216>.
- (22) You, S.; Chen, M.-W.; Dlott, D. D.; Suslick, K. S. Ultrasonic Hammer Produces Hot Spots in Solids. *Nature Comm.* **2015**, *6* (1), 1–7. <https://doi.org/10.1038/ncomms7581>.
- (23) Deidda, C.; Delogu, F.; Cocco, G. In Situ Characterisation of Mechanically-Induced Self-Propagating Reactions. *Journal of Materials Science 2004 39:16* **2004**, *39* (16), 5315–5318. <https://doi.org/10.1023/B:JMSC.0000039236.48464.8F>.
- (24) McKissic, K. S.; Caruso, J. T.; Blair, R. G.; Mack, J. Comparison of Shaking versus Baking: Further Understanding the Energetics of a Mechanochemical Reaction. *Green Chem.* **2014**, *16* (3), 1628–1632. <https://doi.org/10.1039/C3GC41496E>.
- (25) Brekalo, I.; Yuan, W.; Mottillo, C.; Lu, Y.; Zhang, Y.; Casaban, J.; Holman, K. T.; James, S. L.; Duarte, F.; Williams, P. A.; Harris, K. D. M.; Friščić, T. Manometric Real-Time Studies of the Mechanochemical Synthesis of Zeolitic Imidazolate Frameworks. *Chem. Sci.* **2020**, *11* (8), 2141–2147. <https://doi.org/10.1039/C9SC05514B>.
- (26) Halasz, I.; Kimber, S. A. J.; Beldon, P. J.; Belenguer, A. M.; Adams, F.; Honkimäki, V.; Nightingale, R. C.; Dinnebier, R. E.; Friščić, T. In Situ and Real-Time Monitoring of Mechanochemical Milling

- Reactions Using Synchrotron X-Ray Diffraction. *Nature Protocols* **2013**, *8* (9), 1718–1729. <https://doi.org/10.1038/nprot.2013.100>.
- (27) Friščić, T.; Halasz, I.; Beldon, P. J.; Belenguer, A. M.; Adams, F.; Kimber, S. A. J.; Honkimäki, V.; Dinnebier, R. E. Real-Time and in Situ Monitoring of Mechanochemical Milling Reactions. *Nature Chemistry* **2013**, *5* (1), 66–73. <https://doi.org/10.1038/nchem.1505>.
- (28) Oliveira, P. F. M. de; Michalchuk, A. A. L.; Buzanich, A. G.; Bienert, R.; Torresi, R. M.; Camargo, P. H. C.; Emmerling, F. Tandem X-Ray Absorption Spectroscopy and Scattering for in Situ Time-Resolved Monitoring of Gold Nanoparticle Mechanochemical Synthesis. *Chemical Comm.* **2020**, *56* (71), 10329–10332. <https://doi.org/10.1039/D0CC03862H>.
- (29) Katsenis, A. D.; Puškarić, A.; Štrukil, V.; Mottillo, C.; Julien, P. A.; Užarević, K.; Pham, M. H.; Do, T. O.; Kimber, S. A. J.; Lazić, P.; Magdysyuk, O.; Dinnebier, R. E.; Halasz, I.; Friščić, T. In Situ X-Ray Diffraction Monitoring of a Mechanochemical Reaction Reveals a Unique Topology Metal-Organic Framework. *Nature Comm.* **2015**, *6*. <https://doi.org/10.1038/ncomms7662>.
- (30) Julien, P. A.; Užarević, K.; Katsenis, A. D.; Kimber, S. A. J.; Wang, T.; Farha, O. K.; Zhang, Y.; Casaban, J.; Germann, L. S.; Etter, M.; Dinnebier, R. E.; James, S. L.; Halasz, I.; Friščić, T. In Situ Monitoring and Mechanism of the Mechanochemical Formation of a Microporous MOF-74 Framework. *J. Am. Chem. Soc.* **2016**, *138* (9), 2929–2932. <https://doi.org/10.1021/jacs.5b13038>.
- (31) Gracin, D.; Štrukil, V.; Friščić, T.; Halasz, I.; Užarević, K. Laboratory Real-Time and in Situ Monitoring of Mechanochemical Milling Reactions by Raman Spectroscopy. *Angewandte Chemie - International Edition* **2014**, *53* (24), 6193–6197. <https://doi.org/10.1002/anie.201402334>.
- (32) Lukin, S.; Užarević, K.; Halasz, I. Raman Spectroscopy for Real-Time and in Situ Monitoring of Mechanochemical Milling Reactions. *Nat. Protoc.* **2021**, *16* (7), 3492–3521. <https://doi.org/10.1038/s41596-021-00545-x>.
- (33) Batzdorf, L.; Fischer, F.; Wilke, M.; Wenzel, K. J.; Emmerling, F. Direct in Situ Investigation of Milling Reactions Using Combined X-Ray Diffraction and Raman Spectroscopy. *Angewandte Chemie - International Edition* **2015**, *54* (6), 1799–1802. <https://doi.org/10.1002/anie.201409834>.
- (34) Kulla, H.; Haferkamp, S.; Akhmetova, I.; Röllig, M.; Maierhofer, C.; Rademann, K.; Emmerling, F. In Situ Investigations of Mechanochemical One-Pot Syntheses. *Angew. Chem. Int. Ed.* **2018**, *57* (20), 5930–5933. <https://doi.org/10.1002/ANIE.201800147>.
- (35) Julien, P. A.; Germann, L. S.; Titi, H. M.; Etter, M.; Dinnebier, R. E.; Sharma, L.; Baltrusaitis, J.; Friščić, T. In Situ Monitoring of Mechanochemical Synthesis of Calcium Urea Phosphate Fertilizer Cocrystal Reveals Highly Effective Water-Based Autocatalysis. *Chem. Sci.* **2020**, *11* (9), 2350–2355. <https://doi.org/10.1039/C9SC06224F>.
- (36) Kulla, H.; Wilke, M.; Fischer, F.; Röllig, M.; Maierhofer, C.; Emmerling, F. Warming up for Mechanochemical Synthesis – Temperature Development in Ball Mills during Synthesis. *Chem. Comm.* **2017**, *53* (10), 1664–1667. <https://doi.org/10.1039/C6CC08950J>.
- (37) Užarević, K.; Štrukil, V.; Mottillo, C.; Julien, P. A.; Puškarić, A.; Friščić, T.; Halasz, I. Exploring the Effect of Temperature on a Mechanochemical Reaction by in Situ Synchrotron Powder X-Ray

- Diffraction. *Cryst. Growth Des.* **2016**, *16* (4), 2342–2347.
<https://doi.org/10.1021/ACS.CGD.6B00137>.
- (38) Michalchuk, A. A. L.; Tumanov, I. A.; Konar, S.; Kimber, S. A. J.; Pulham, C. R.; Boldyreva, E. v. Challenges of Mechanochemistry: Is In Situ Real-Time Quantitative Phase Analysis Always Reliable? A Case Study of Organic Salt Formation. *Adv. Sci.* **2017**, *4* (9), 1700132.
<https://doi.org/10.1002/advs.201700132>.
- (39) Singh, K.; Blümich, B. NMR Spectroscopy with Compact Instruments. *TrAC - Trends Anal. Chem.* **2016**, *83*, 12–26. <https://doi.org/10.1016/j.trac.2016.02.014>.
- (40) Brown, S. P. Applications of High-Resolution ¹H Solid-State NMR. *Solid State Nucl. Magn. Reson.* **2011**, *41*, 1–27. <https://doi.org/10.1016/j.ssnmr.2011.11.006>.
- (41) Taylor, A. J.; Salerno, M.; Dharmakumar, R.; Jerosch-Herold, M. T1 Mapping Basic Techniques and Clinical Applications. *JACC: Cardiovasc. Imaging* **2016**, *9*, 67–81.
<https://doi.org/10.1016/j.jcmg.2015.11.005>.
- (42) Dong, Z.; Andrews, T.; Xie, C.; Yokoo, T. Advances in MRI Techniques and Applications. *BioMed Res. Int.* **2015**, *2015*, 1–2. <https://doi.org/10.1155/2015/139043>.
- (43) Mitchell, J.; Chandrasekera, T. C.; Holland, D. J.; Gladden, L. F.; Fordham, E. J. Magnetic Resonance Imaging in Laboratory Petrophysical Core Analysis. *Phys. Rep.* **2013**, *526* (3), 165–225.
<https://doi.org/10.1016/j.physrep.2013.01.003>.
- (44) Coates, G. R.; Xiao, L.; Prammer, M. G. *NMR Logging Principles and Applications*, 1st ed.; Halliburton Energy Services, Ed.; Gulf Publishing Company: Houston, 1999.
- (45) Chen, Q.; Marble, A. E.; Colpitts, B. G.; Balcom, B. J. The Internal Magnetic Field Distribution, and Single Exponential Magnetic Resonance Free Induction Decay, in Rocks. *J. Magn. Reson.* **2005**, *175* (2), 300–308. <https://doi.org/10.1016/j.jmr.2005.05.001>.
- (46) Marangoni, A. G.; Macmillan, B.; Marty, S.; Balcom, B. J. Spatial Mapping of Solid and Liquid Lipid in Chocolate. In *Magn. Res. Food Sci.*; 2009; pp 105–112.
- (47) Hemdane, S.; Jacobs, P. J.; Bosmans, G. M.; Verspreet, J.; Delcour, J. A.; Courtin, C. M. Study of Biopolymer Mobility and Water Dynamics in Wheat Bran Using Time-Domain ¹H NMR Relaxometry. *Food Chem.* **2017**, *236*, 68–75. <https://doi.org/10.1016/j.foodchem.2017.01.020>.
- (48) Troutman, M. Y.; Mastikhin, I. v.; Balcom, B. J.; Eads, T. M.; Ziegler, G. R. Moisture Migration in Soft-Panned Confections during Engrossing and Aging as Observed by Magnetic Resonance Imaging. *J. Food Eng.* **2001**, *48* (3), 257–267. [https://doi.org/10.1016/S0260-8774\(00\)00167-9](https://doi.org/10.1016/S0260-8774(00)00167-9).
- (49) Mariette, F. Investigations of Food Colloids by NMR and MRI. *Curr. Opin. Colloid Interface Sci.* **2009**, *14* (3), 203–211. <https://doi.org/10.1016/j.cocis.2008.10.006>.
- (50) Marreiros, J. O.; de Oliveira-Silva, R.; Iacomi, P.; Llewellyn, P. L.; Ameloot, R.; Sakellariou, D. Benchtop In Situ Measurement of Full Adsorption Isotherms by NMR. *J. Am. Chem. Soc.* **2021**, *143*, 8249–8254. <https://doi.org/10.1021/jacs.1c03716>.

- (51) Enjilela, R.; Guo, J.; MacMillan, B.; Marica, F.; Afrough, A.; Balcom, B. T1-T2* Relaxation Correlation Measurements. *J. Magn. Res.* **2021**, *326*, 106961. <https://doi.org/10.1016/j.jmr.2021.106961>.
- (52) Zamiri, M. S.; MacMillan, B.; Marica, F.; Guo, J.; Romero-Zerón, L.; Balcom, B. J. Petrophysical and Geochemical Evaluation of Shales Using Magnetic Resonance T1-T2* Relaxation Correlation. *Fuel* **2021**, *284*, 119014. <https://doi.org/10.1016/j.fuel.2020.119014>.
- (53) Zamiri, M. S.; Florea, M.; Romero-Zerón, L.; Balcom, B. J. Monitoring Shale Water Uptake Using 2D Magnetic Resonance Relaxation Correlation and SPRITE MRI. *Chem. Eng. J.* **2021**, *428*, 131042-undefined. <https://doi.org/https://doi.org/10.1016/j.cej.2021.131042>.
- (54) Guo, J.; Macmillan, B.; Sadegh Zamiri, M.; Balcom, B. J. Two Dimensional 1 H Magnetic Resonance Relaxometry-Based Analyses of Argonne Premium Coals. *Fuel* **2021**, *302*, 121106. <https://doi.org/10.1016/j.fuel.2021.121106>.
- (55) Zhou, H.-C.; Long, J. R.; Yaghi, O. M. Introduction to Metal–Organic Frameworks. *Chem. Rev.* **2012**, *112* (2), 673–674. <https://doi.org/10.1021/CR300014X>.
- (56) Furukawa, H.; Cordova, K. E.; O’Keeffe, M.; Yaghi, O. M. The Chemistry and Applications of Metal–Organic Frameworks. *Science* **2013**, *341* (6149). <https://doi.org/10.1126/SCIENCE.1230444>.
- (57) Yuan, S.; Feng, L.; Wang, K.; Pang, J.; Bosch, M.; Lollar, C.; Sun, Y.; Qin, J.; Yang, X.; Zhang, P.; Wang, Q.; Zou, L.; Zhang, Y.; Zhang, L.; Fang, Y.; Li, J.; Zhou, H.-C. Stable Metal–Organic Frameworks: Design, Synthesis, and Applications. *Adv. Mater.* **2018**, *30* (37), 1704303. <https://doi.org/10.1002/ADMA.201704303>.
- (58) Friščić, T.; Reid, D. G.; Halasz, I.; Stein, R. S.; Dinnebier, R. E.; Duer, M. J. Ion- and Liquid-Assisted Grinding: Improved Mechanochemical Synthesis of Metal–Organic Frameworks Reveals Salt Inclusion and Anion Templating. *Angew. Chem. Int. Ed.* **2010**, *49* (4), 712–715. <https://doi.org/10.1002/ANIE.200906583>.
- (59) Główniak, S.; Szczęśniak, B.; Choma, J.; Jaroniec, M. Mechanochemistry: Toward Green Synthesis of Metal–Organic Frameworks. *Mater. Today* **2021**, *46*, 109–124. <https://doi.org/10.1016/J.MATTOD.2021.01.008>.
- (60) Stolar, T.; Užarević, K. Mechanochemistry: An Efficient and Versatile Toolbox for Synthesis, Transformation, and Functionalization of Porous Metal–Organic Frameworks. *CrystEngComm* **2020**, *22* (27), 4511–4525. <https://doi.org/10.1039/D0CE00091D>.
- (61) Pichon, A.; Lazuen-Garay, A.; James, S. L. Solvent-Free Synthesis of a Microporous Metal–Organic Framework. *CrystEngComm* **2006**, *8* (3), 211–214. <https://doi.org/10.1039/B513750K>.
- (62) Garay, A. L.; Pichon, A.; James, S. L. Solvent-Free Synthesis of Metal Complexes. *Chem. Soc. Rev.* **2007**, *36* (6), 846–855. <https://doi.org/10.1039/B600363J>.
- (63) Ma, X.; Yuan, W.; Bell, S. E. J.; James, S. L. Better Understanding of Mechanochemical Reactions: Raman Monitoring Reveals Surprisingly Simple ‘Pseudo-Fluid’ Model for a Ball Milling Reaction. *Chem. Comm.* **2014**, *50* (13), 1585–1587. <https://doi.org/10.1039/C3CC47898J>.

- (64) Aboutorabi, L.; Morsali, A. Structural Transformations and Solid-State Reactivity Involving Nano Lead(II) Coordination Polymers via Thermal, Mechanochemical and Photochemical Approaches. *Coord. Chem. Rev.* **2016**, *310*, 116–130. <https://doi.org/10.1016/J.CCR.2015.10.006>.
- (65) Fujii, K.; Garay, A. L.; Hill, J.; Sbircea, E.; Pan, Z.; Xu, M.; Apperley, D. C.; James, S. L.; Harris, K. D. M. Direct Structure Elucidation by Powder X-Ray Diffraction of a Metal–Organic Framework Material Prepared by Solvent-Free Grinding. *Chem. Comm.* **2010**, *46* (40), 7572–7574. <https://doi.org/10.1039/C0CC02635B>.
- (66) Crawford, D.; Casaban, J.; Haydon, R.; Giri, N.; McNally, T.; James, S. L. Synthesis by Extrusion: Continuous, Large-Scale Preparation of MOFs Using Little or No Solvent. *Chem. Sci.* **2015**, *6* (3), 1645–1649. <https://doi.org/10.1039/C4SC03217A>.
- (67) Park, K. S.; Ni, Z.; Côté, A. P.; Choi, J. Y.; Huang, R.; Uribe-Romo, F. J.; Chae, H. K.; O’Keeffe, M.; Yaghi, O. M. Exceptional Chemical and Thermal Stability of Zeolitic Imidazolate Frameworks. *PNAS* **2006**, *103* (27), 10186–10191. <https://doi.org/10.1073/pnas.0602439103>.
- (68) Rosi, N. L.; Kim, J.; Eddaoudi, M.; Chen, B.; O’Keeffe, M.; Yaghi, O. M. Rod Packings and Metal–Organic Frameworks Constructed from Rod-Shaped Secondary Building Units. *J. Am. Chem. Soc.* **2005**, *127* (5), 1504–1518. <https://doi.org/10.1021/JA045123O>.
- (69) Garzón-Tovar, L.; Carné-Sánchez, A.; Carbonell, C.; Imaz, I.; Maspoch, D. Optimised Room Temperature, Water-Based Synthesis of CPO-27-M Metal–Organic Frameworks with High Space-Time Yields. *J. Mater. Chem. A* **2015**, *3* (41), 20819–20826. <https://doi.org/10.1039/C5TA04923G>.
- (70) Mason, J. A.; Sumida, K.; Herm, Z. R.; Krishna, R.; Long, Jeffrey. R. Evaluating Metal–Organic Frameworks for Post-Combustion Carbon Dioxide Capture via Temperature Swing Adsorption. *Energy Environ. Sci.* **2011**, *4* (8), 3030–3040. <https://doi.org/10.1039/C1EE01720A>.
- (71) Jin, C. X.; Shang, H. B. Synthetic Methods, Properties and Controlling Roles of Synthetic Parameters of Zeolite Imidazole Framework-8: A Review. *J. Solid State Chem.* **2021**, *297*, 122040. <https://doi.org/10.1016/J.JSSC.2021.122040>.
- (72) Guo, J.; MacMillan, B.; Zamiri, M. S.; Balcom, B. J. Magnetic Resonance T1–T2* and T1ρ–T2* Relaxation Correlation Measurements in Solid-like Materials with Non-Exponential Decays. *J. Magn. Res.* **2021**, *328*, 107005. <https://doi.org/10.1016/j.jmr.2021.107005>.
- (73) Beldon, P. J.; Fábíán, L.; Stein, R. S.; Thirumurugan, A.; Cheetham, A. K.; Frišćić, T. Rapid Room-Temperature Synthesis of Zeolitic Imidazolate Frameworks by Using Mechanochemistry. *Angew. Chem. Int. Ed.* **2010**, *49* (50), 9640–9643. <https://doi.org/10.1002/ANIE.201005547>.
- (74) Frišćić, T.; Childs, S. L.; Rizvi, S. A. A.; Jones, W. The Role of Solvent in Mechanochemical and Sonochemical Cocrystal Formation: A Solubility-Based Approach for Predicting Cocrystallisation Outcome. *CrystEngComm* **2009**, *11* (3), 418–426. <https://doi.org/10.1039/B815174A>.
- (75) Xiao, T.; Liu, D. The Most Advanced Synthesis and a Wide Range of Applications of MOF-74 and Its Derivatives. *Micropor. Mesopor. Mat.* **2019**, *283*, 88–103. <https://doi.org/10.1016/j.micromeso.2019.03.002>.

- (76) Tanaka, S.; Nagaoka, T.; Yasuyoshi, A.; Hasegawa, Y.; Denayer, J. F. M. Hierarchical Pore Development of ZIF-8 MOF by Simple Salt-Assisted Mechanochemistry. *Cryst. Growth Des.* **2018**, *18* (1), 274–279. <https://doi.org/10.1021/acs.cgd.7b01211>.
- (77) BP, H.; DE, C.; L, G.; P, H.; SL, J. Feedback Kinetics in Mechanochemistry: The Importance of Cohesive States. *Angew. Chem. Int. Ed.* **2017**, *56* (48), 15252–15256. <https://doi.org/10.1002/ANIE.201706723>.
- (78) Rô Me Canivet, J.; Fateeva, A.; Guo, Y.; Coasne, B.; Farrusseng, D. Water Adsorption in MOFs: Fundamentals and Applications. *Chem. Soc. Rev.* **2014**, *43* (16), 5594–5617. <https://doi.org/10.1039/c4cs00078a>.
- (79) Lowe, I. J.; Norberg, R. E. Free-Induction Decays in Solids. *Phys. Rev.* **1957**, *107*, 46–61. <https://doi.org/10.1103/PhysRev.107.46>.
- (80) Derbyshire, W.; van den Bosch, M.; van Dusschoten, D.; MacNaughtan, W.; Farhat, I. A.; Hemminga, M. A.; Mitchell, J. R. Fitting of the Beat Pattern Observed in NMR Free-Induction Decay Signals of Concentrated Carbohydrate-Water Solutions. *J. Magn. Res.* **2004**, *168* (2), 278–283. <https://doi.org/10.1016/j.jmr.2004.03.013>.

Relaxation Time Correlation NMR for Mechanochemical Reaction

Monitoring of Metal-Organic Frameworks

Madeleine E. Leger^{ab}, Jiangfeng Guo^b, Bryce MacMillan^b, Hatem M. Titi^c, Tomislav Friščić^c, Barry A. Blight^{a}, and Bruce Balcom^{a,b*}.*

^a Department of Chemistry, University of New Brunswick, Fredericton, New Brunswick, E3B 5A3, Canada

^b UNB MRI Centre, Department of Physics, University of New Brunswick, Fredericton, New Brunswick, E3B 5A3, Canada

^c Department of Chemistry, McGill University, Montreal, Quebec, H3A 0G4, Canada

* Corresponding author: bjb@unb.ca, b.blight@unb.ca

Supplementary Material

Table of Contents

S1: Experimental	S2-S3
S2: Relaxation Time Values	S4-S5
S3: 1D Relaxation Time Plots	S6-13
S4: Non-Exponential Relaxation Time Correlation Plots	S14-S15
S5: PRXD Analysis	S16
S6: SEM and EDS Analysis	S17-S20
S7: TGA Analysis	S21
S8: References	S22

S1: Methods

Probe and Teflon vials



Figure S1. Doty DS1-874 ^1H RF probe, small 7.5 mL Teflon jar, and two small 7 mm zirconia balls.

PXRD

The identities of the all reactants were confirmed through X-ray powder patterns that were collected on a Bruker D8 Advance spectrometer in the UNB geochemical and spectrographic facilities. Fine powder samples (gently crushed in mortar when necessary) were packed into the circular well on the sample-holder, after which it was placed on the sample stage and scanned. The diffractometer was equipped with a two circle (theta-theta) goniometer housed in a radiation safety enclosure. The X-ray source was a sealed, 2.2 kW Cu X-ray tube, maintained at an operating current of 40 kV and 25 mA. The X-ray optics was that of standard Bragg-Brentano para-focusing mode with the X-rays diverging from a divergence slit (1.00 mm) at the tube to strike the sample and then converging through an anti-scatter receiving slit (1.00 mm) and a detector slit (0.20 mm). The goniometer was computer controlled with independent stepper motors and optical encoders for the θ and 2θ circles with the smallest angular step size of $0.0001^\circ 2\theta$. Samples were scanned in the range of $5-70^\circ 2\theta$. A step size of 0.02° and a step time of 1.0 sec were used during the measurements. A peltier-cooled solid-state [Si(Li)] detector (Sol-X) with a useful energy range of 1 to 60 KeV was used as the detector. No correction was made for K_β radiation. A set of 2° Soller slits were used in order to lower horizontal beam divergence.

The identities of the after-milling products were obtained on a Bruker D2 PHASER diffractometer equipped with a LynxEye linear position sensitive detector (Bruker AXS, Madison, WI, USA), using Ni-filtered $\text{CuK}\alpha$ radiation. The data were collected between 2θ $4-50^\circ$, at increment of 0.02° and exposure time of 0.3 s.

SEM/EDS

SEM images and EDS data were collected on a JEOL JSM-6400 Scanning Electron Microscope equipped with an EDAX Genesis 4000 Energy Dispersive X-ray (EDS) analyser at the UNB Microscopy and Microanalysis Facility. EDS analysis was performed at an

accelerating voltage of 15 kV and a beam current of 1.5 nA, with a working distance of 14 mm. Collection time was 50 seconds per analysis point.

TGA

TGA data were obtained on a TGA 5500 Discovery by TA Instruments. The samples were heated to 700°C at a rate of 10 °C/min and a gas flow of 25 mL/min.

MR measurement

Solid materials have particularly interesting T_1 - T_2^* behaviors. Solids commonly feature very long T_1 values and extremely short T_2 values. This is explained by Bloembergen-Purcell-Pound (BPP) theory which illustrates the theoretical relationship between T_1 and T_2 relaxation times and molecular mobility.¹ BPP theory emphasizes the importance of correlation time and motion in determining MR lifetime. Solids have increasingly large T_1 values as molecular and proton mobility decreases, and very short T_2 values. Since T_2^* decay is governed by T_2 , the T_2^* decay of solids is very short. Indeed, in our study, a T_1 of 47.7 s and a T_2^* as short as 5.7 μ s were measured.

These unusual relaxation times heavily influenced our relaxation measurement and pulse sequence choices. Common relaxation time methodologies to obtain T_1 - T_2 data based on multiple spin echoes are not appropriate for solid samples since the short-lived signal decays too rapidly compared to the echo time and long 90° and 180° pulses. A typical pulse sequence to obtain bulk T_1 - T_2^* data employs inversion recovery, with FIDs acquired as a function of recovery time. This sequence is problematic since the minimum observation time of the sequence is too long to observe the short-lived T_2^* signal.

To keep the measurements in this study straightforward, we utilized a saturation recovery pulse sequence to obtain T_1 - T_2^* data. Saturation recovery (figure 4b) is the most appropriate MR sequence for solid-state analysis for a few reasons. First, it is a quick measurement. There is no need to wait five times the value of T_1 or to use a full 90° pulse during the sequence, which greatly reduces the minimum observation time of the sequence. Also, saturation recovery allows the measurement of very short T_2^* decays because of the lack of multiple spin echoes or long RF pulses. To assure the acquisition of the short-lived FID decay, a short duration RF pulse, 5 μ s, was utilized in this study. It is also important to have short acquisition deadtimes to have a chance at measuring the very short T_2^* component. The deadtime (dt) was 4 μ s.

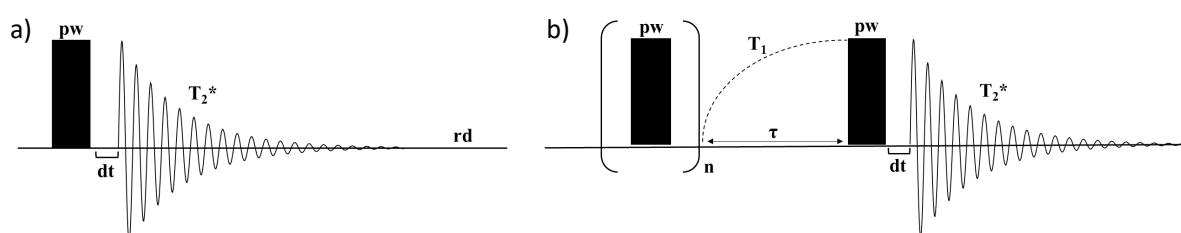
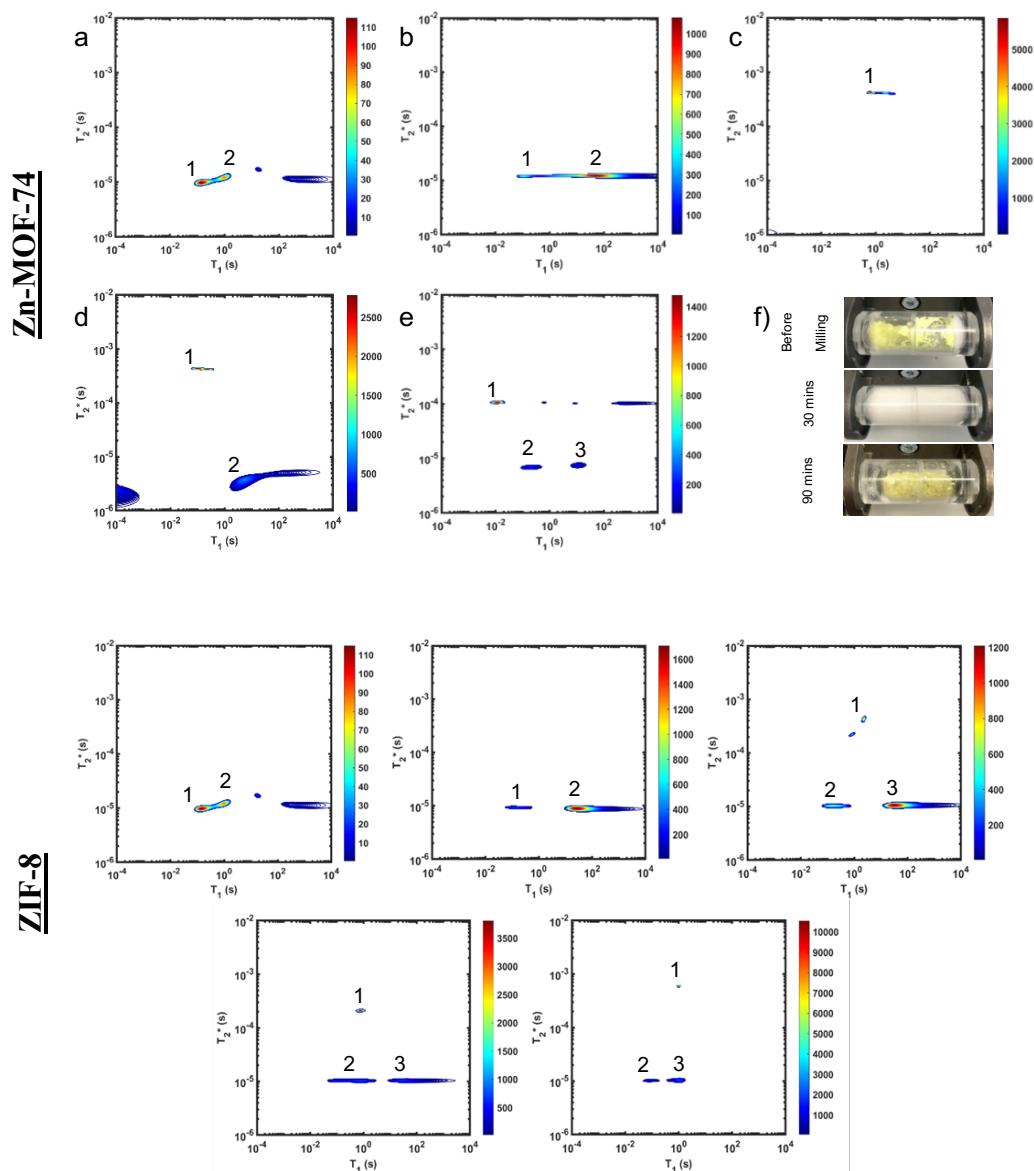


Figure S2. The pulse sequence of a (a) FID and (b) saturation recovery with some important parameters shown. The pulse width (pw) and probe dead time (dt) must be kept short to ensure capturing short-lived signal from the solid samples. In the FID sequence, the recycle delay (rd) is an important factor in measurement time since its value should be equal to five times the value of the longest T_1 in the sample. In the saturation recovery sequence, a series (n) of pw pulses are applied followed by a series of different lengths of recovery times (τ). The T_2^* values are obtained from the FID curves, while the T_1 weighing depends on the longitudinal magnetization recovery after saturation.

S2: Relaxation Time Values

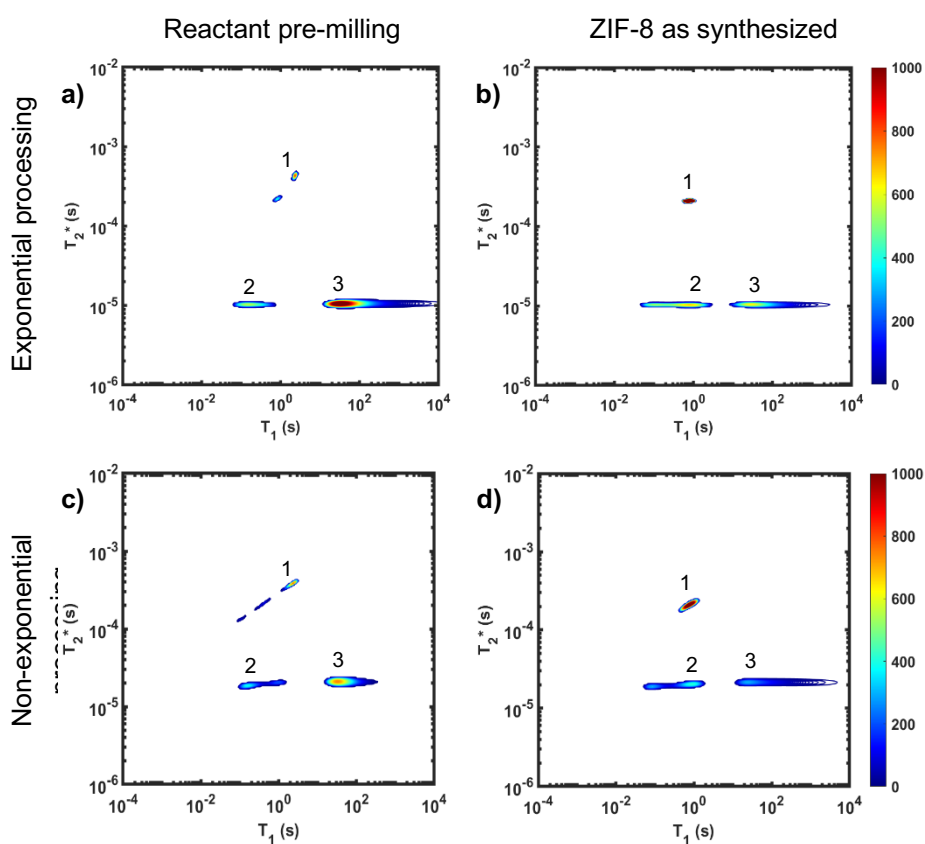
	Sample	Peak		
		1	2	3
		$(T_1, T_2^*) /$		
		$(s, \mu s)$		
Zn-MOF-74	Zinc oxide	(0.14, 9.7)	(0.96, 12.1)	
	2,5-dihydroxyterephthalic acid	(0.11, 12.1)	(47.7, 12.1)	
	Before milling	(0.63, 416)		
	Milling 30 minutes	(0.10, 432)	(7.29, 4.09)	
	After milling	(0.012, 106)	(0.20, 6.8)	(11.2, 7.6)
ZIF-8	Zinc oxide	(0.14, 9.7)	(0.96, 12.1)	
	2-methylimidazole	(0.17, 9.1)	(24.9, 9.1)	
	Before milling	(2.30, 432)	(0.15, 10.5)	(30.9, 10.5)
	After milling	(0.78, 210)	(0.83, 10.5)	(28.8, 10.5)
	After milling rinsed	(1.04, 598)	(0.08, 10.1)	(1.04, 10.5)

Table S1. Relaxation times of ZIF-8 and MOF-74 synthesis. (corresponding numbered plots below)



	Sample	Peak	1	2	3
		$(T_1, T_2^*) /$ (s, μ s)			
Exp.	Reactants pre-milling		(2.30, 432)	(0.15, 10.5)	(30.9, 10.5)
	ZIF-8 as synthesized		(0.78, 210)	(0.83, 10.5)	(28.8, 10.5)
Non-Exp.	Reactants pre-milling		(2.30, 387)	(0.16, 18.6)	(33.2, 20.8)
	ZIF-8 as synthesized		(0.78, 210)	(0.90, 20.0)	(24.9, 21.5)

Table S2. Relaxation times of ZIF-8 synthesis comparing exponential and non-exponential processing. (corresponding numbered plots below)



S3: 1D Relaxation Time Plots

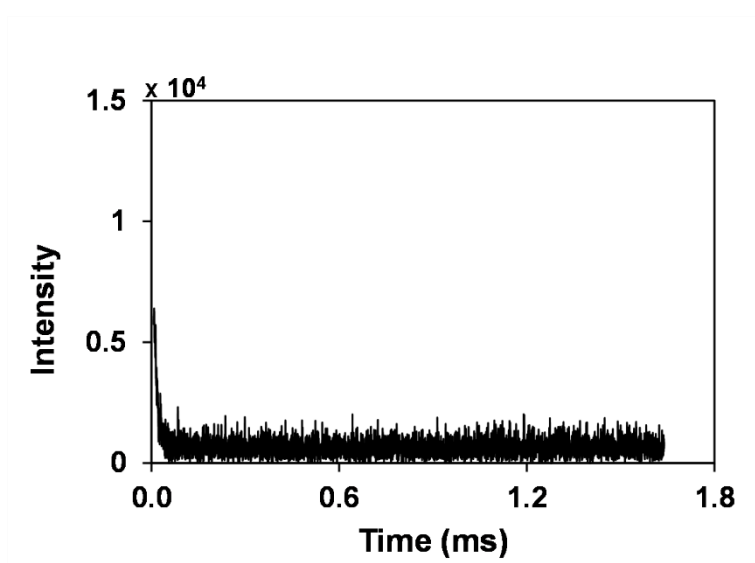


Figure S3. Free induction decay (FID) measurement of T_2^* in zinc oxide sample.

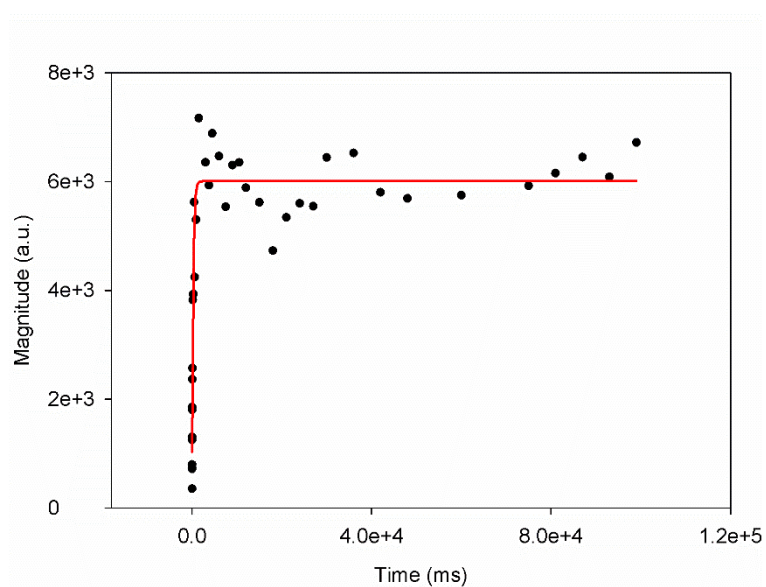


Figure S4. Saturation recovery measurement of T_1 in zinc oxide sample.

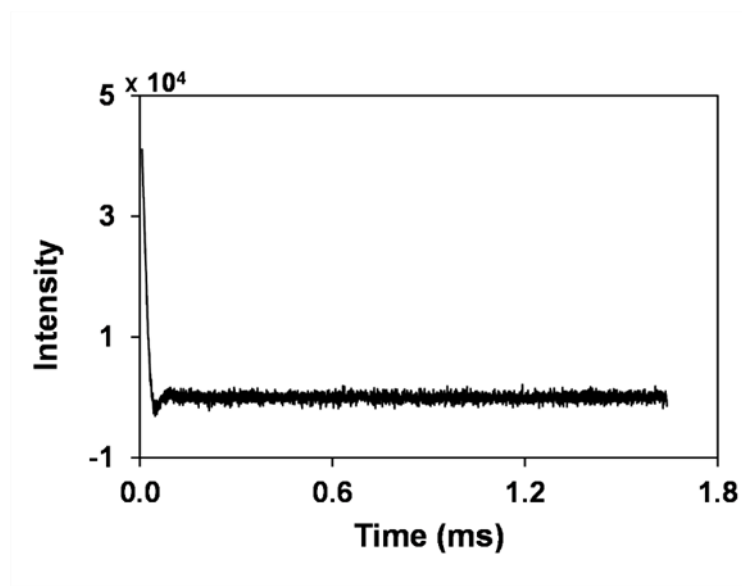


Figure S5. Free induction decay (FID) measurement of T_2^* in 2,5-dihydroxyterephthalic acid sample.

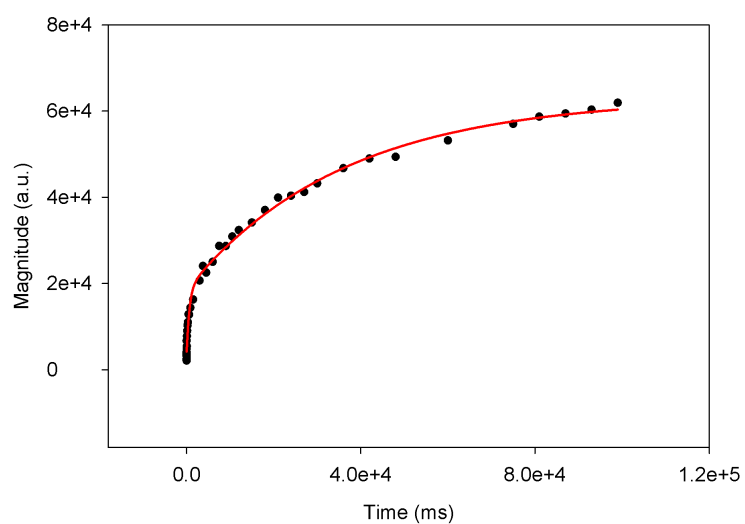


Figure S6. Saturation recovery measurement of T_1 in 2,5-dihydroxyterephthalic acid sample.

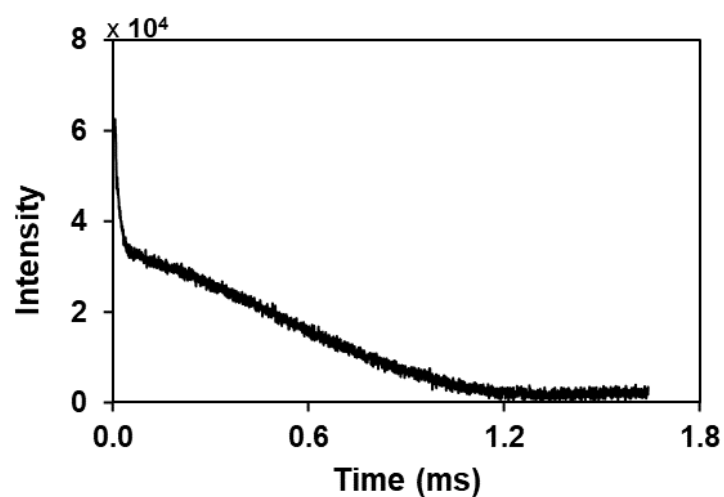


Figure S7. Free induction decay (FID) measurement of T_2^* in Zn-MOF-74 mixture before milling sample.

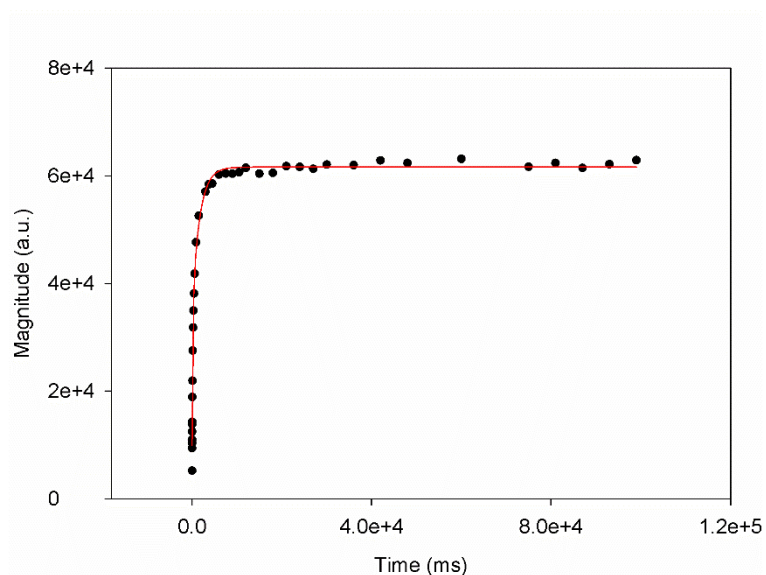


Figure S8. Saturation recovery measurement of T_1 in Zn-MOF-74 mixture before milling sample.

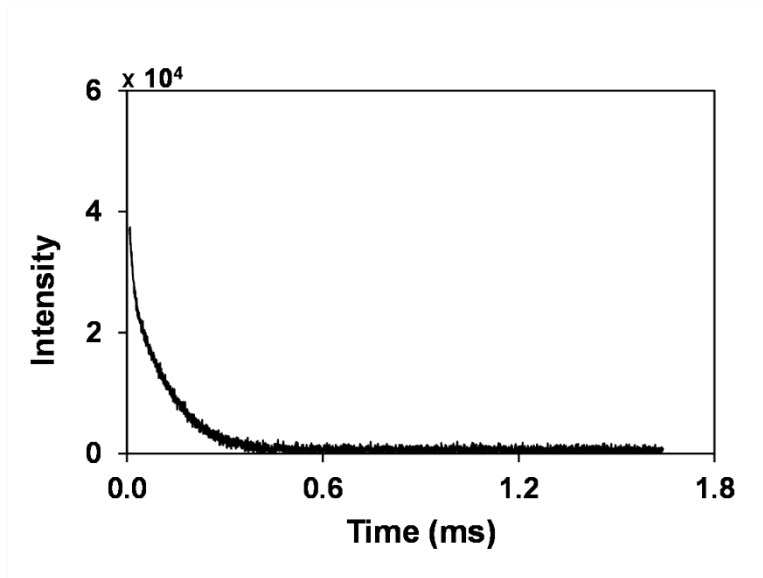


Figure S9. Free induction decay (FID) measurement of T_2^* in Zn-MOF-74 as synthesized sample.

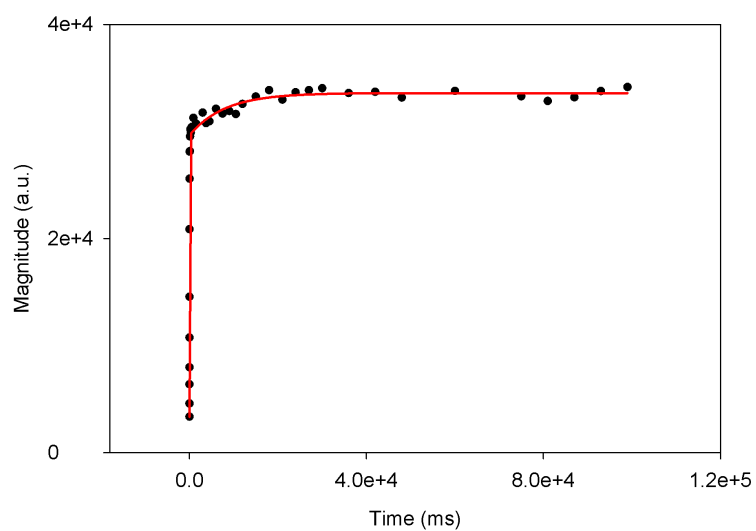


Figure S10. Saturation recovery measurement of T_1 in Zn-MOF-74 as synthesized sample.

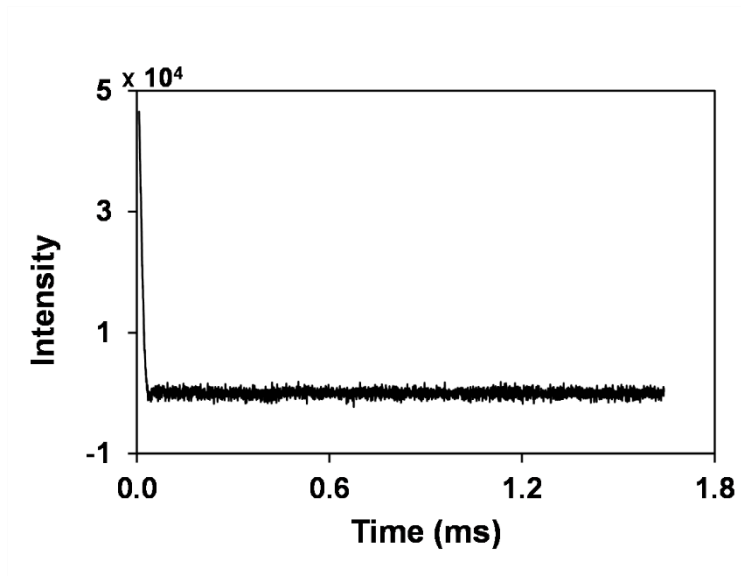


Figure S11. Free induction decay (FID) measurement of T_2^* in 2-methylimidazole sample.

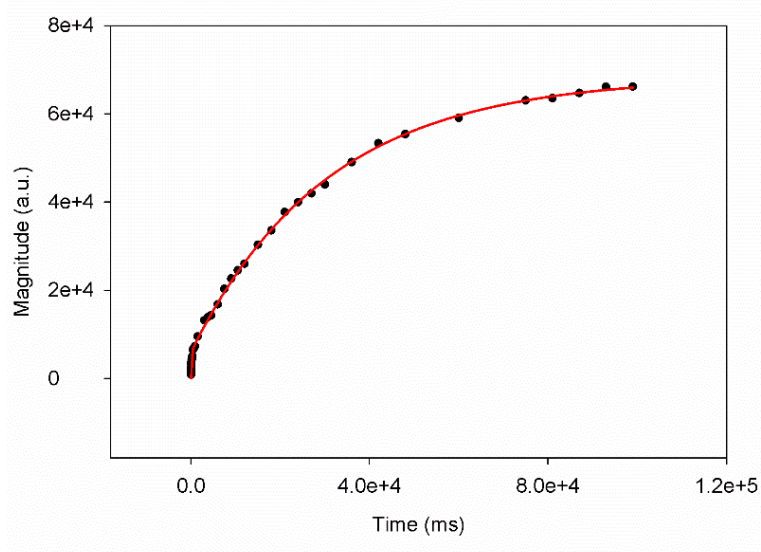


Figure S12. Saturation recovery measurement of T_1 in 2-methylimidazole sample.

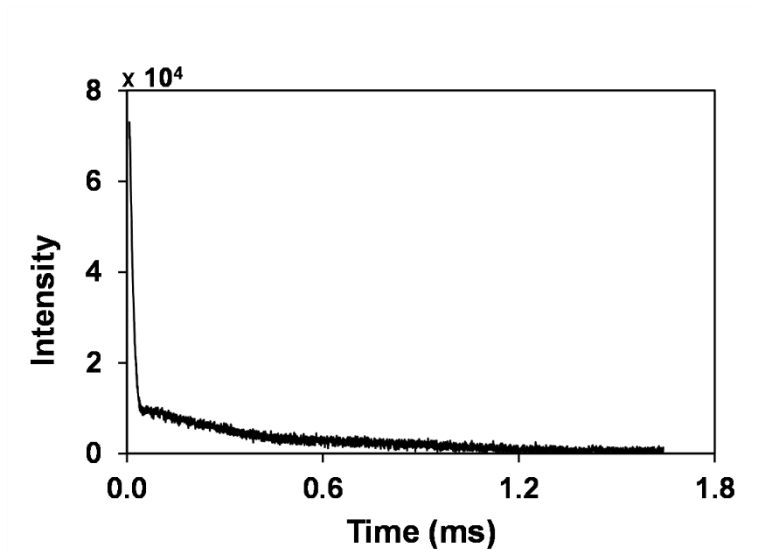


Figure S13. Free induction decay (FID) measurement of T_2^* in ZIF-8 mixture before milling sample.

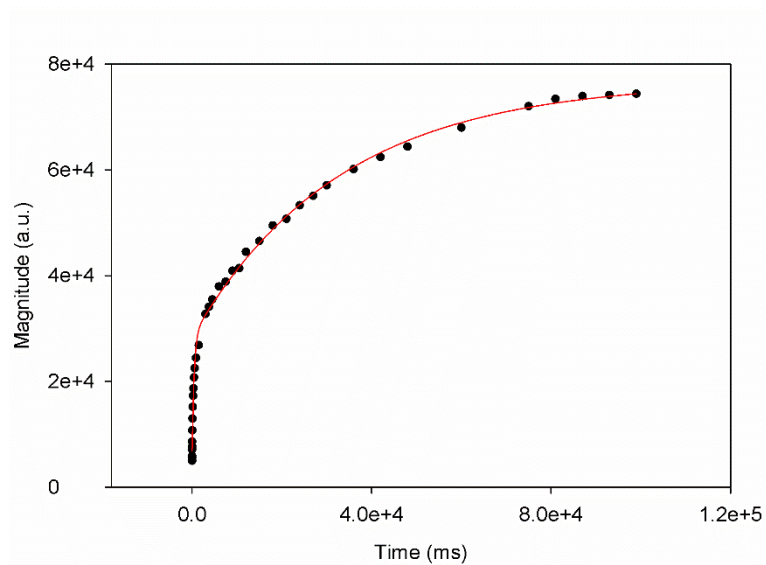


Figure S14. Saturation recovery measurement of T_1 in ZIF-8 mixture before milling sample.

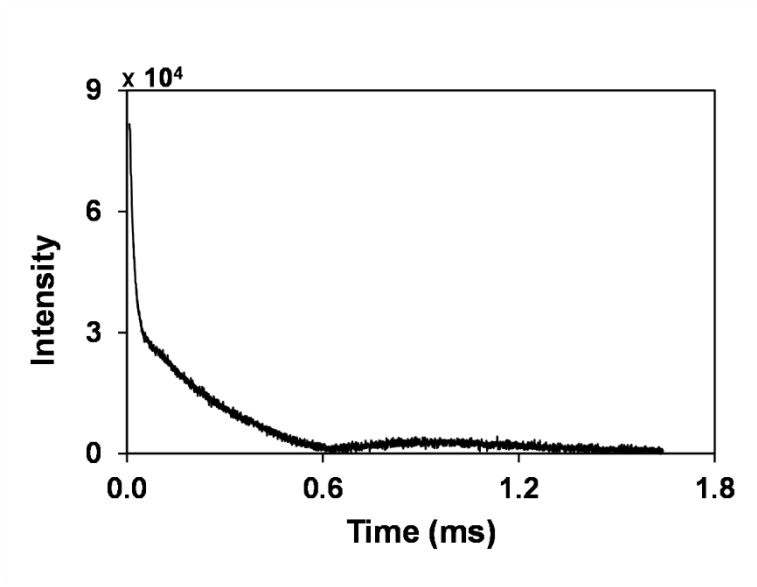


Figure S15. Free induction decay (FID) measurement of T_2^* in ZIF-8 as synthesized sample.

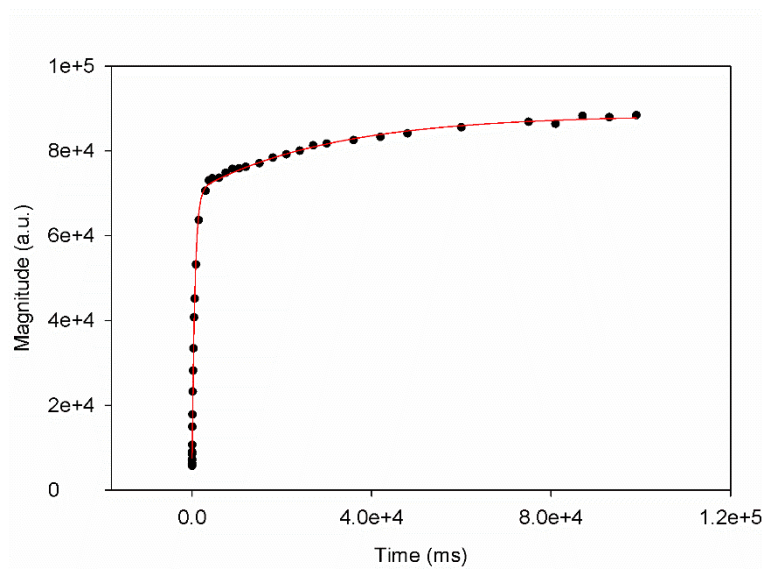


Figure S16. Saturation recovery measurement of T_1 in ZIF-8 as synthesized sample.

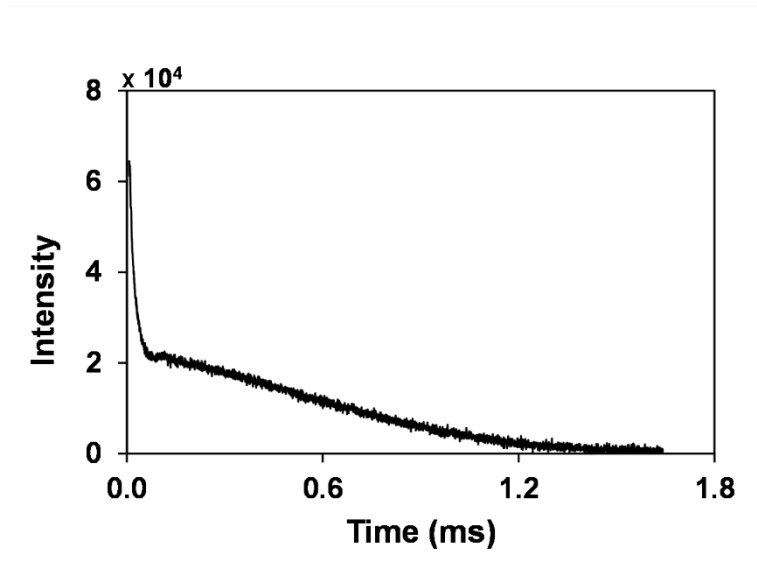


Figure S17. Free induction decay (FID) measurement of T_2^* in ZIF-8 rinsed and dried sample.

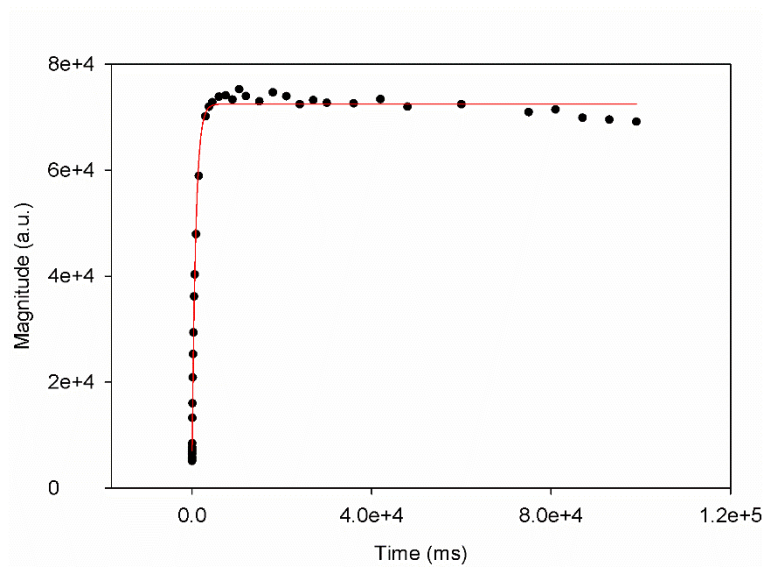


Figure S18. Saturation recovery measurement of T_1 in ZIF-8 rinsed and dried sample.

S4: Non-Exponential Relaxation Time Correlation Plots

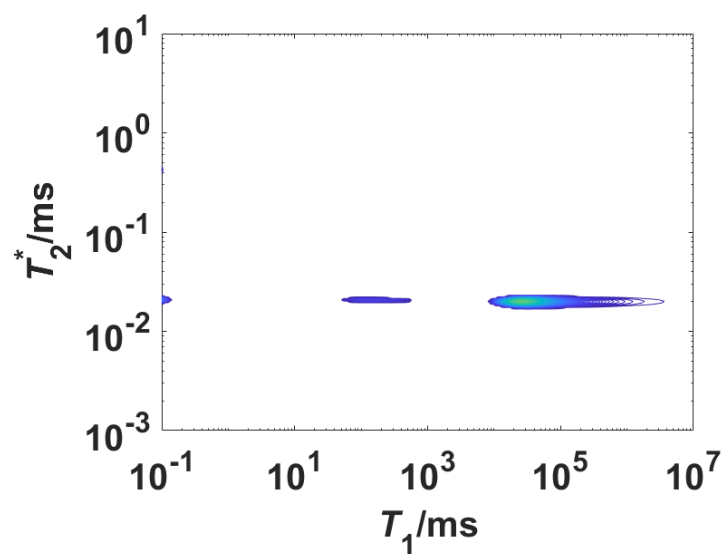


Figure S19. T_1 - T_2^* correlation plot of 2-methylimidazole, using non-exponential processing.

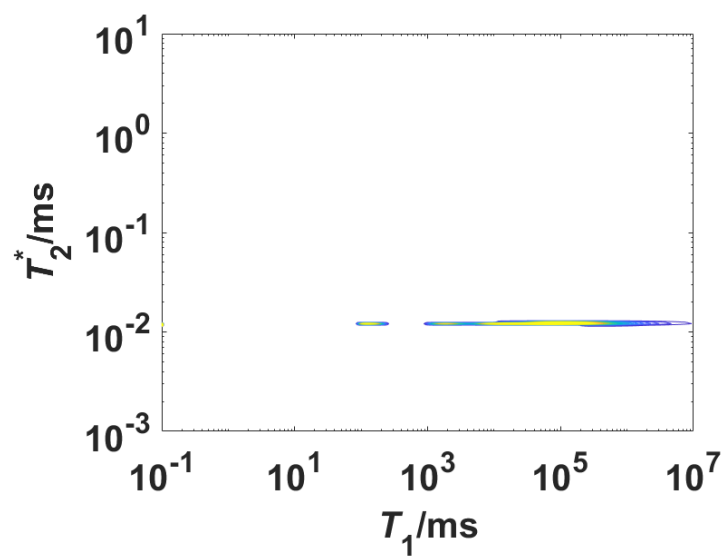


Figure S20. T_1 - T_2^* correlation plot of 2,5-dihydroxyterephthalic acid, using non-exponential processing.

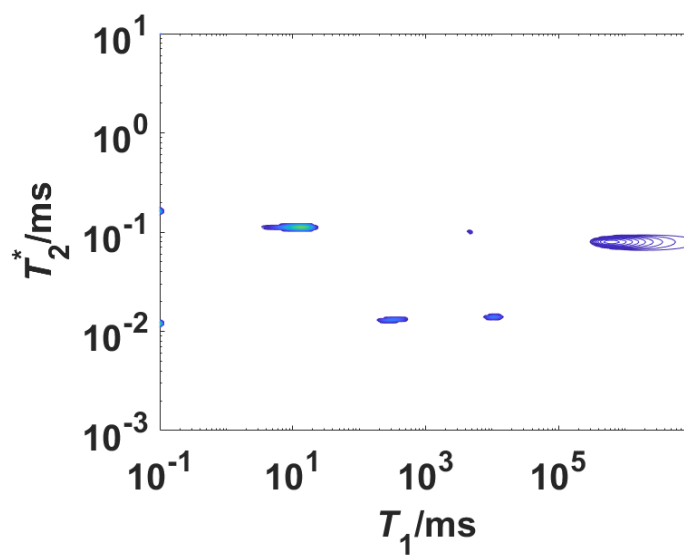


Figure S21. T_1 - T_2^* correlation plot of Zn-MOF-74 after milling, using non-exponential processing.

S5: PXRD Analysis

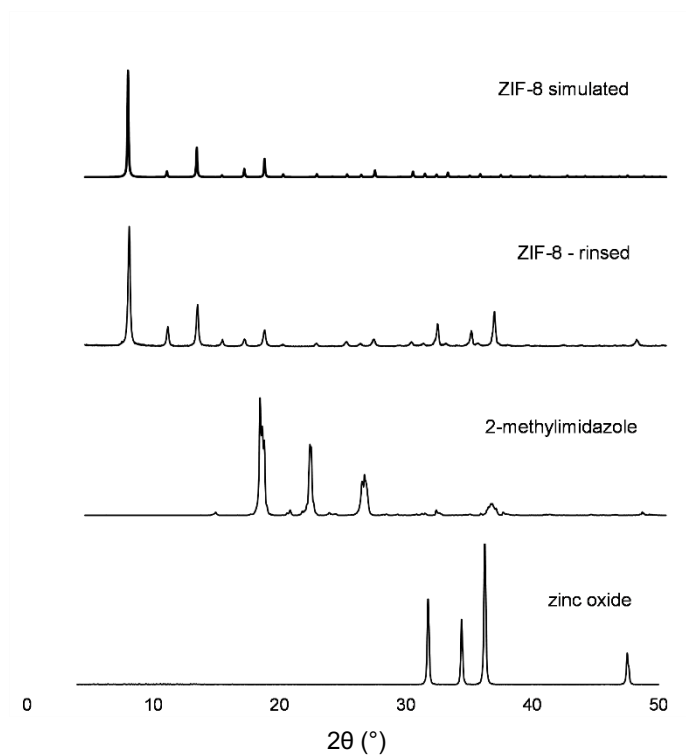


Figure S22. PXRD data of the ZIF-8 reaction. Simulated data obtained using Mercury.²

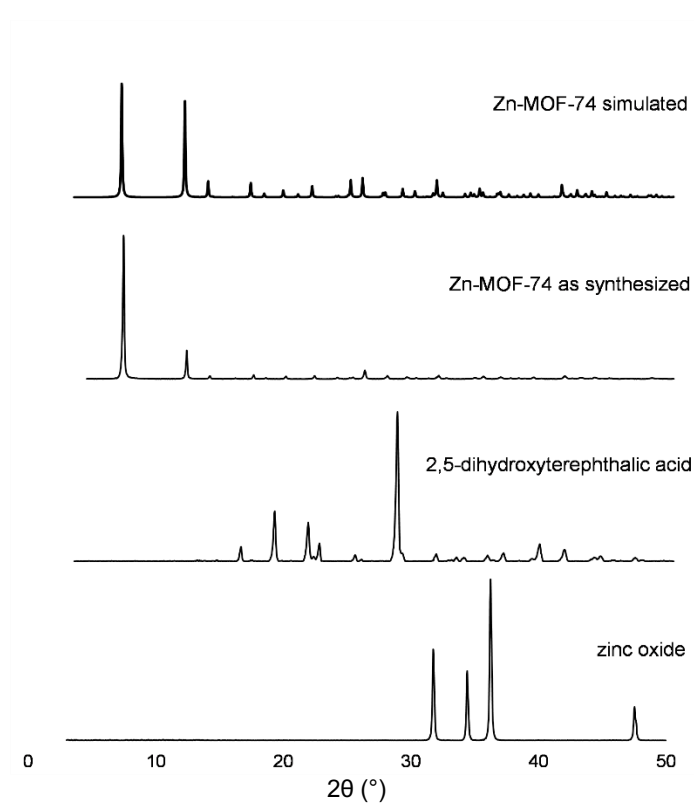


Figure S23. PXRD data of the Zn-MOF-74 reaction. Simulated data obtained using Mercury.²

S6: SEM and EDS Analysis

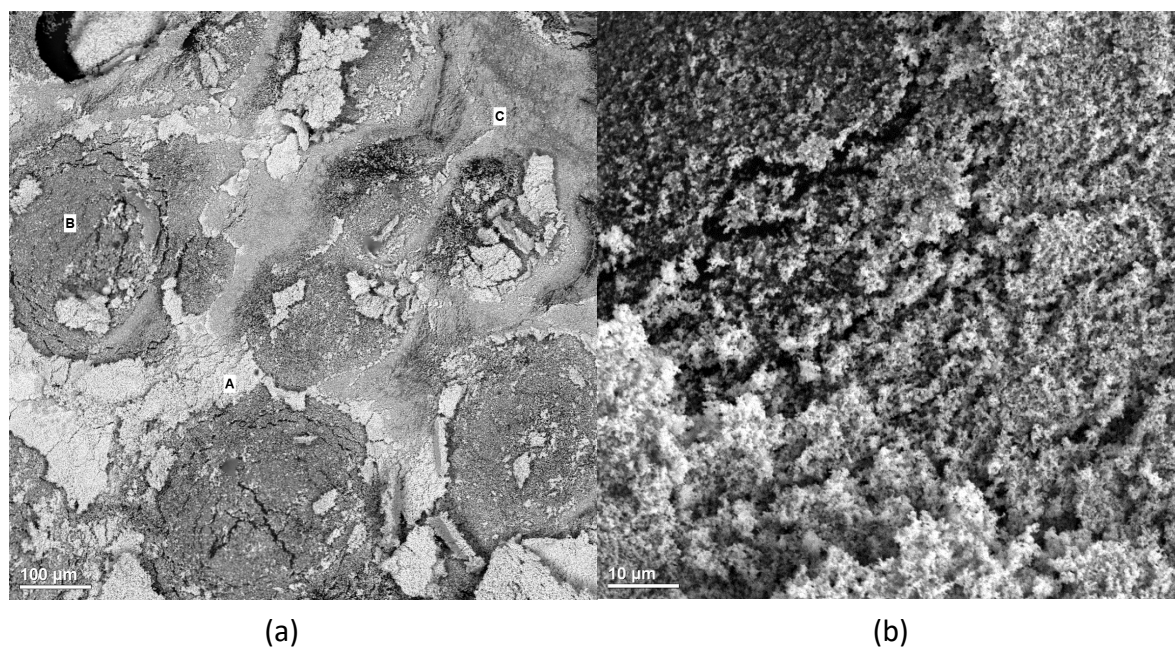


Figure S24. SEM micrographs of zinc oxide at 100 μm (a) and 10 μm (b).

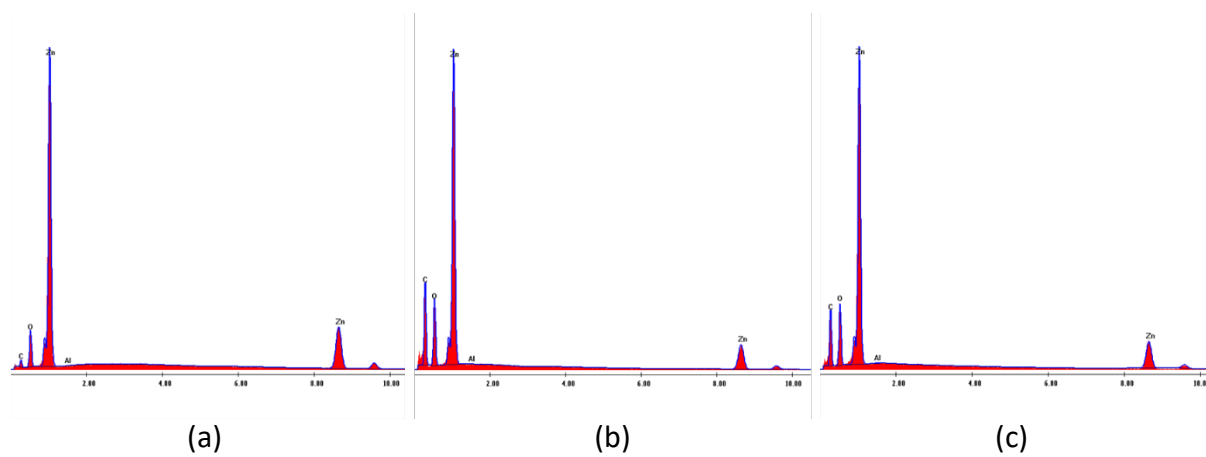


Figure S25. EDS analysis of zinc oxide (figure S24a, 100 μm).

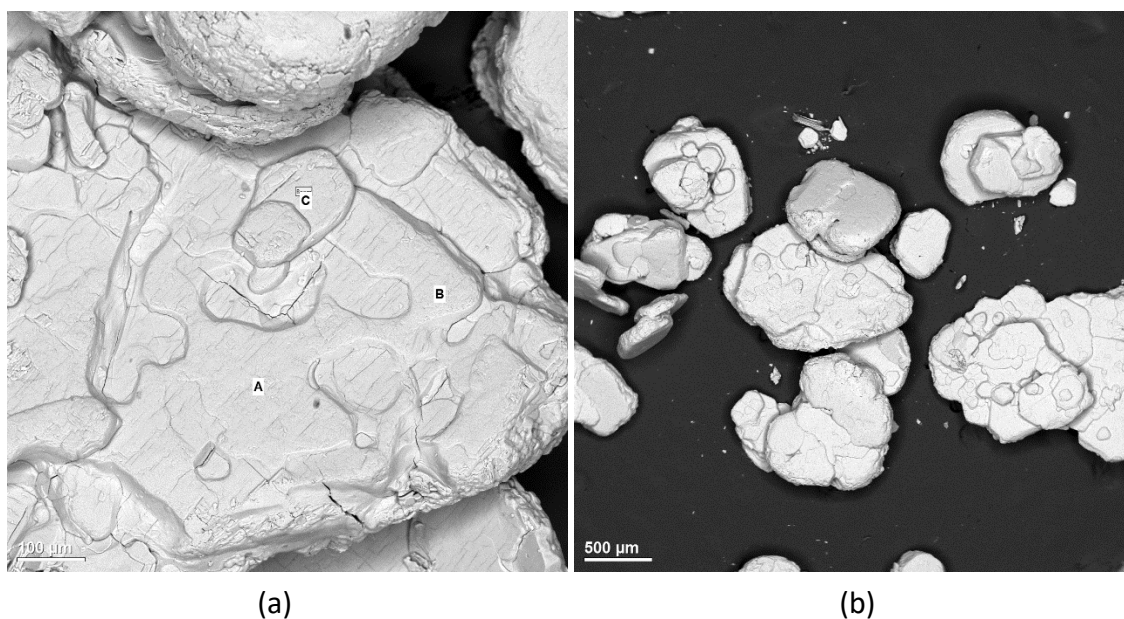


Figure S26. SEM micrographs of zinc acetate dihydrate at 100 μm (a) and 500 μm (b).

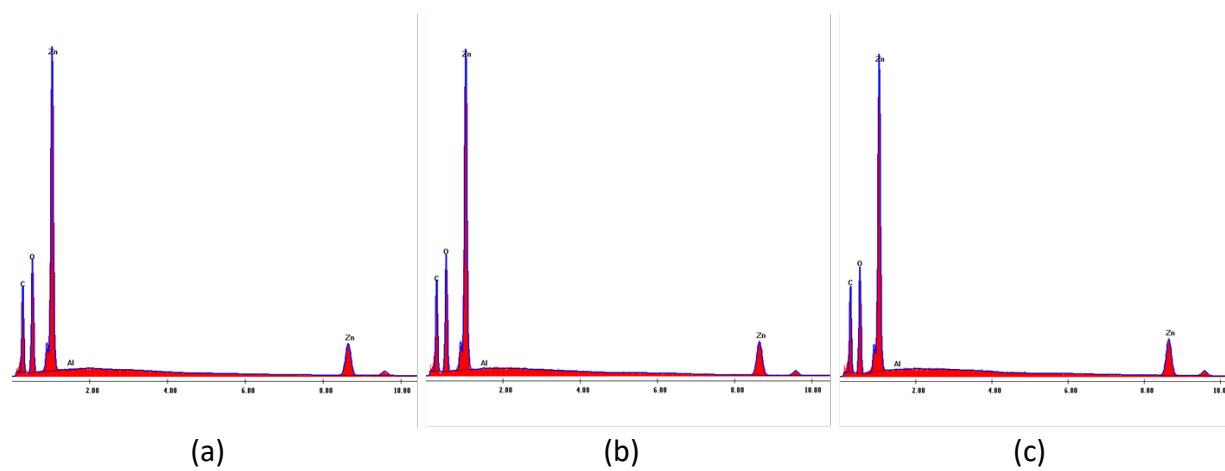


Figure S27. EDS analysis of zinc acetate dihydrate (figure S26a, 100 μm).

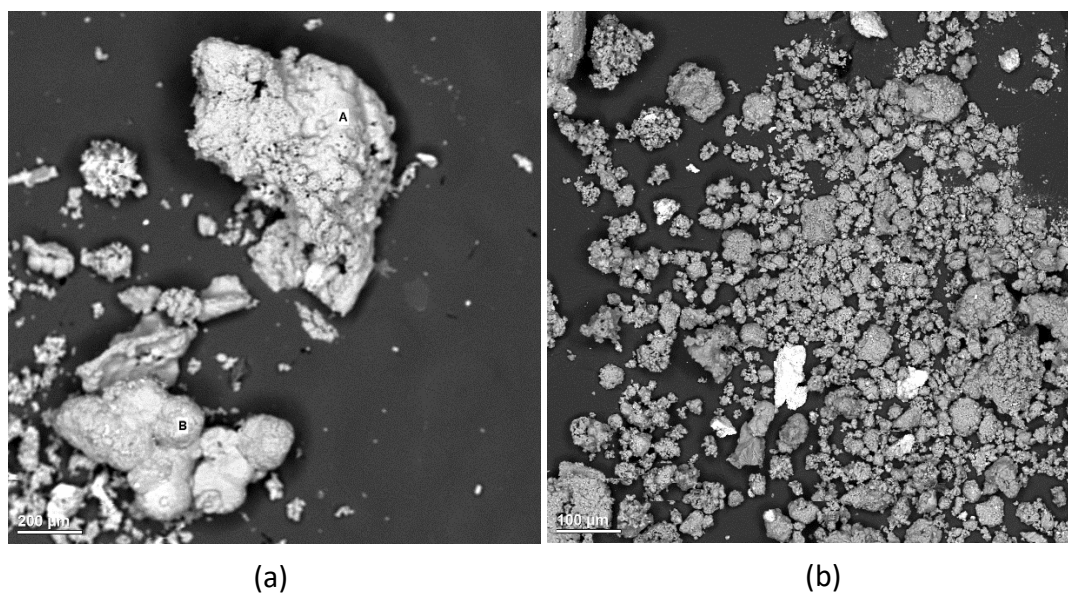


Figure S28. SEM micrographs of ZIF-8 after milling at 200 μm (a) and 100 μm (b).

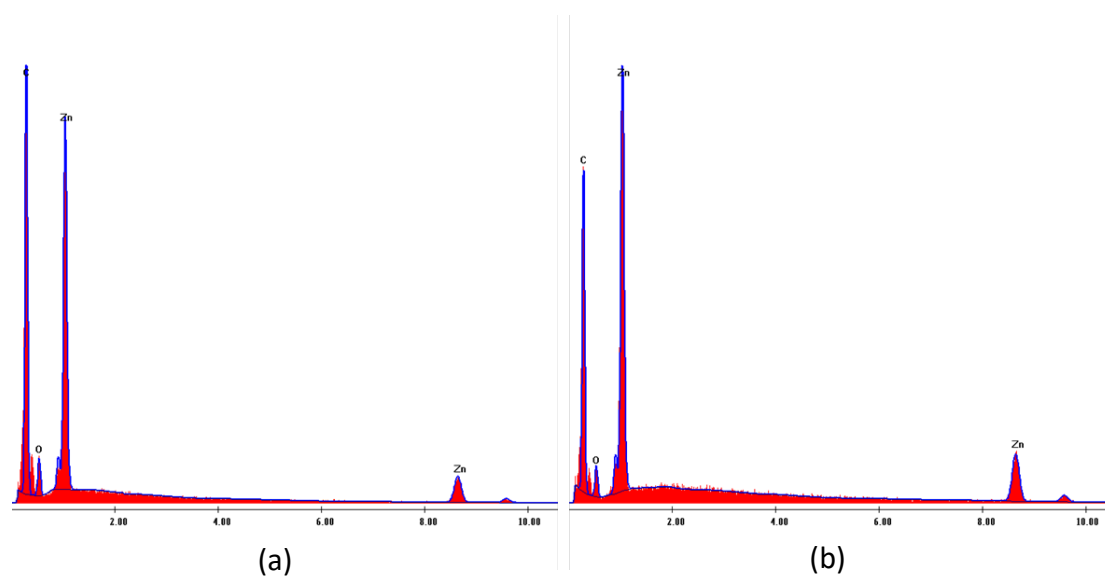


Figure S29. EDS analysis of ZIF-8 (figure S28a, 200 μm).

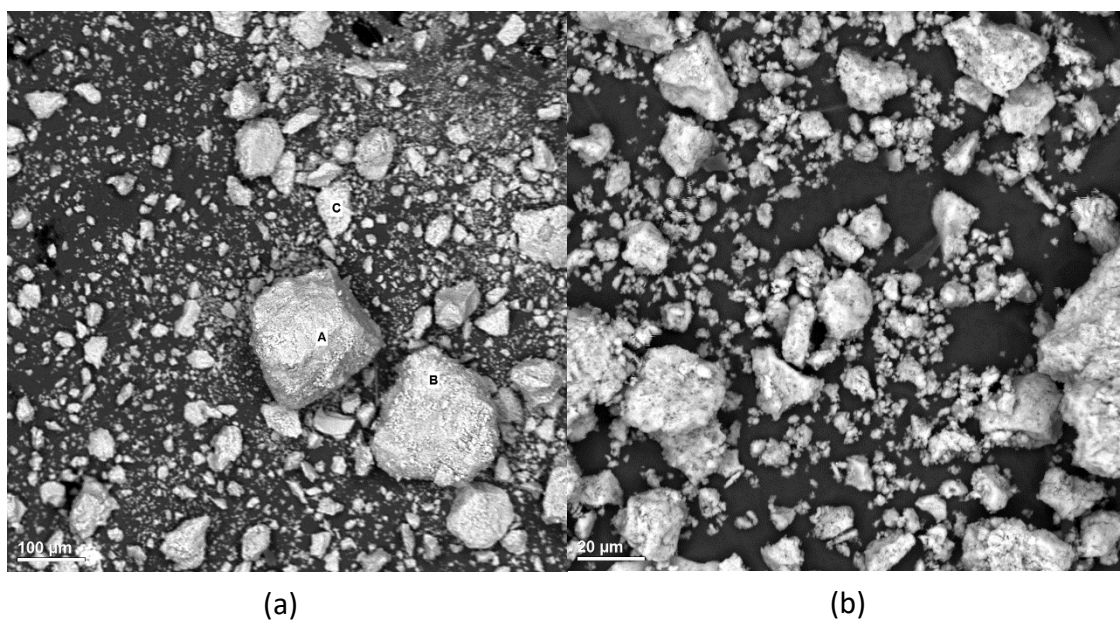


Figure S30. SEM micrographs of Zn-MOF-74 after milling at 100 μm (a) and 20 μm (b).

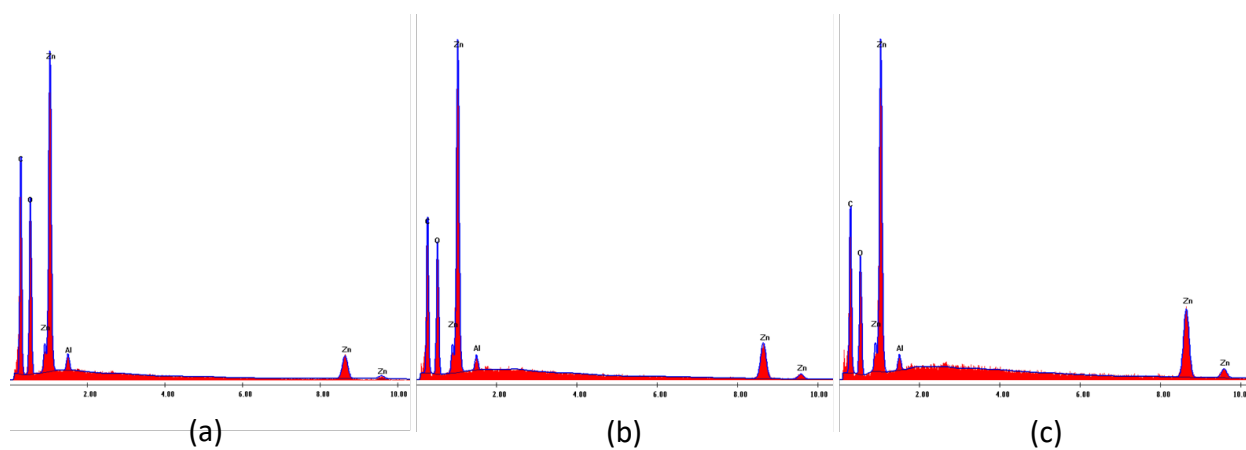


Figure S31. EDS analysis of Zn-MOF-74 (figure S30a, 100 μm).

S7: TGA Analysis

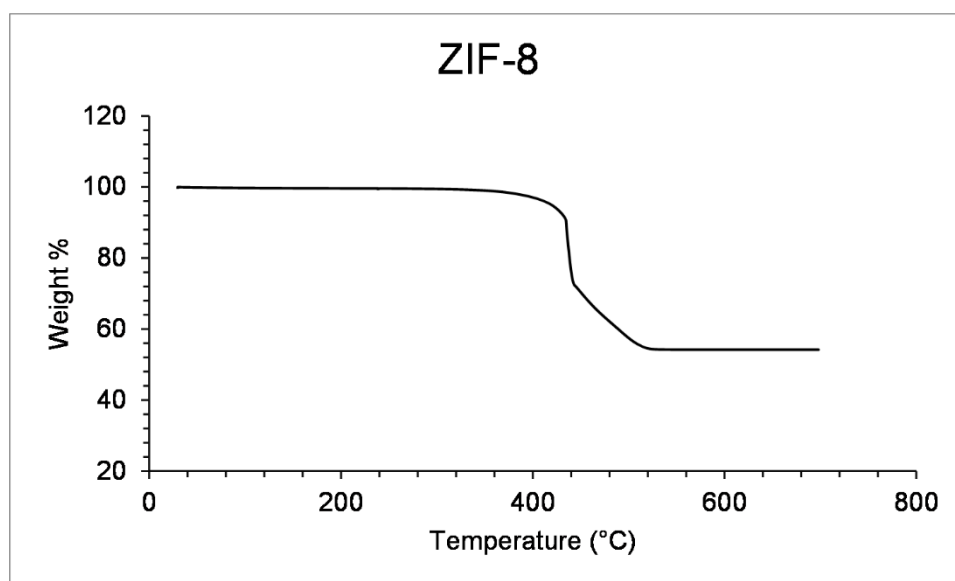


Figure S32. TGA analysis of ZIF-8.

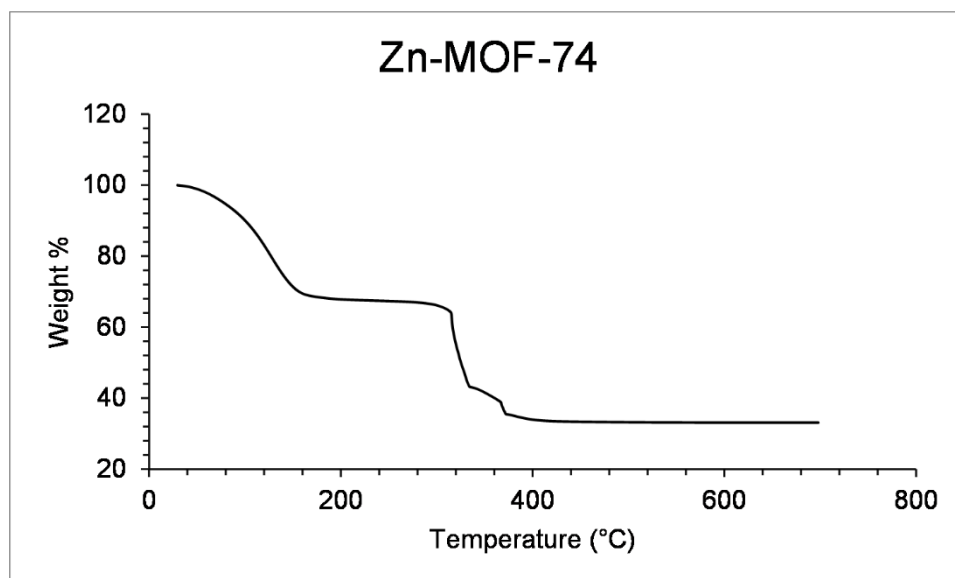


Figure S33. TGA analysis of Zn-MOF-74.

S8: References

- (1) Bloembergen, N.; Purcell, E. M.; Pound, R. v. Relaxation Effects in Nuclear Magnetic Resonance Absorption. *Phys. Rev.* **1948**, *73* (7), 679–712. <https://doi.org/10.1103/PhysRev.73.679>.
- (2) Macrae, C. F.; Sovago, I.; Cottrell, S. J.; Galek, P. T. A.; McCabe, P.; Pidcock, E.; Platings, M.; Shields, G. P.; Stevens, J. S.; Towler, M.; Wood, P. A.; IUCr. Mercury 4.0: From Visualization to Analysis, Design and Prediction. *J. Appl. Cryst.* **2020**, *53*, 226–235. <https://doi.org/10.1107/S1600576719014092>.